

The poorly constrained cluster disruption time-scale in the Large Magellanic Cloud

Geneviève Parmentier^{1,2*} † ‡ § and Richard de Grijs^{3,4}

¹*Argelander Institute for Astronomy, University of Bonn, Auf dem Hugel, D-53121 Bonn, Germany*

²*Institute of Astrophysics & Geophysics, University of Liège, 17 avenue du 6 Août, B-4000 Liège, Belgium*

³*Department of Physics & Astronomy, The University of Sheffield, Hicks Building, Hounsfield Road, Sheffield S3 7RH, UK*

⁴*National Astronomical Observatories, Chinese Academy of Sciences, 20A Datun Road, Chaoyang District, Beijing 100012, P. R. China*

Accepted 2007 October 16. Received 2007 October 05; in original form 2007 August 16

ABSTRACT

We use Monte-Carlo simulations, combined with homogeneously determined age and mass distributions based on multi-wavelength photometry, to constrain the cluster formation history and the rate of bound cluster disruption in the Large Magellanic Cloud (LMC) star cluster system. We evolve synthetic star cluster systems formed with a power-law initial cluster mass function (ICMF) of spectral index $\alpha = -2$ assuming different cluster disruption time-scales. For each of these cluster disruption time-scales we derive the corresponding cluster formation rate (CFR) required to reproduce the observed cluster age distribution. We then compare, in a “Poissonian” χ^2 sense, model mass distributions and model two-dimensional distributions in $\log(\text{mass})$ vs. $\log(\text{age})$ space of the detected surviving clusters to the observations. Because of the bright detection limit ($M_V^{\text{lim}} \simeq -4.7$ mag) above which the observed cluster sample is complete, one cannot constrain the characteristic cluster disruption time-scale for a $10^4 M_\odot$ cluster, t_4^{dis} (where the disruption time-scale depends on cluster mass as $t_{\text{dis}} = t_4^{\text{dis}}(M_{\text{cl}}/10^4 M_\odot)^\gamma$, with $\gamma \simeq 0.62$), to better than a lower limit, $t_4^{\text{dis}} \geq 1$ Gyr.

We conclude that the CFR has been increasing steadily from 0.3 clusters Myr^{-1} 5 Gyr ago, to a present rate of (20 – 30) clusters Myr^{-1} , for clusters spanning a mass range of $\sim 100 - 10^7 M_\odot$. For older ages the derived CFR depends sensitively on our assumption of the underlying CMF shape. If we assume a universal Gaussian ICMF, then the CFR has increased steadily over a Hubble time from ~ 1 cluster Gyr^{-1} 15 Gyr ago to its present value. On the other hand, if the ICMF has always been a power law with a slope close to $\alpha = -2$, the CFR exhibits a minimum some 5 Gyr ago, which we tentatively identify with the well-known age gap in the LMC’s cluster age distribution.

Key words: globular clusters: general – galaxies: kinematics and dynamics – Magellanic Clouds – galaxies: star clusters

1 INTRODUCTION

The mass and age distributions of star cluster systems contain the (fossil) records of their formation conditions. They are therefore among the best tracers of the star-formation histories of their host galaxies available to observers. It is important to realise, however, that one needs to understand both the dominant internal and external evolutionary processes in order to disentangle this formation record, and

hence obtain a glimpse of the initial conditions required for star cluster formation.

The effects of stellar evolution in a given star cluster (which can be approximated by a “simple” stellar population once the cluster has reached an age that is well in excess of its formation time-scale) are rather well understood, whereas we have only recently begun to make major *quantitative* inroads into understanding the environmental effects leading to star cluster “weight loss” (i.e., the preferential depletion of the low-mass component of the cluster’s stellar mass function caused by tidal stripping and the ejection of stars owing to internal two-body relaxation) and – eventually – disruption.

Estimates of the characteristic cluster disruption time-

* E-mail: gparm@astro.uni-bonn.de

† Humboldt Research Fellow

‡ Research Fellow of Belgian Science Policy

§ Honorary Scientific Research Worker of *Fonds National de la Recherche Scientifique*, Belgium

scales in various star cluster environments have been calculated by Boutloukos & Lamers (2003), de Grijs et al. (2003a,b,c), Gieles et al. (2005) and de Grijs & Anders (2006), among others (see also Lamers et al. 2005a,b). Specifically, Boutloukos & Lamers (2003) and Lamers et al. (2005b) show that the cluster age distribution and cluster mass function approximate a double power law when a cluster system is affected by both fading and secular dynamical evolution. Knowledge of the detection limit in terms of cluster mass vs. age, combined with the estimate of the cluster age or mass at the “break point” of the integrated cluster age (mass) distribution (see, e.g., fig. 1 in Boutloukos & Lamers 2003, where the “break points” are referred to as t_{cross} and M_{cross} in the age and mass distributions, respectively) then leads to the typical cluster disruption time-scale. Their analysis, however, explicitly builds on the assumption of a constant cluster formation rate (CFR, i.e. the number of clusters formed per linear time interval dN/dt is constant in time) as a function of time. In that context, the (poorly-known) time-variable CFR of the LMC cluster system hampers such an analysis. If only the observed cluster age distribution is known, then we are left with a degeneracy between the CFR and the disruption time-scale, in the sense that one cannot distinguish between a low CFR combined with slow secular dynamical evolution on the one hand, and a vigorous CFR combined with cluster disruption occurring on a rapid time-scale on the other.

The star cluster system in the Large Magellanic Cloud (LMC) has the potential of providing strong constraints to the theory of star cluster disruption as a function of environment, since it is composed of the largest resolved cluster system spanning *both* a reasonable mass range ($\sim 10^2 - 10^6 M_{\odot}$; cf. Hunter et al. 2003, hereafter H03; de Grijs & Anders 2006, and references therein) *and* an age range from a few Myr to ~ 13 Gyr available. In addition, thanks to the LMC’s proximity, we have been able to obtain observations – and derived the age and mass distributions – of a sufficiently large cluster sample to allow a statistical approach to its evolution (e.g., H03; de Grijs & Anders 2006; see also Sect. 2).

On the basis of the few star clusters systems analysed in detail to date, including M51 and the Antennae interacting system, Bastian et al. (2005), Fall et al. (2005) and Fall (2006) suggest that the early evolution of star cluster systems is most likely characterised by a rapid, largely mass-independent “infant mortality” phase, at least for masses $\gtrsim 10^4 M_{\odot}$ (see also de Grijs & Parmentier 2007; and references therein), combined with “infant weight loss” (the loss of stars caused by rapid, early gas expulsion; cf. Weidner et al. 2007), the effects of which are enhanced by stellar evolutionary mass loss. In this scenario, this early phase, which ends when clusters reach an age of ~ 40 to 50 Myr (e.g., Goodwin & Bastian 2006), would then be followed by (mass-dependent) secular evolution. The early, rapid cluster disruption process results from the expulsion of the intra-cluster gas due to adiabatic or explosive expansion driven by stellar winds or supernova activity (Mengel et al. 2005; Bastian & Goodwin 2006; Goodwin & Bastian 2006; see de Grijs & Parmentier 2007 for a review). Star clusters are expected to settle back into virial equilibrium ~ 40 to 50 Myr after gas expulsion (Goodwin & Bastian 2006). In our analysis in this paper we will therefore exclude star clusters younger than

50 Myr, since our main purpose is to derive the characteristic (mass-dependent) time-scale of cluster disruption in the LMC driven by secular evolution only. In a follow-up paper (Goodwin et al., in prep.), we will discuss the evolution of the LMC cluster system on the shortest time-scales relevant to the infant mortality and infant weight loss scenarios.

In de Grijs & Anders (2006), we found that the LMC’s CFR has been roughly constant outside of the well-known age gap between ~ 3 and 13 Gyr, when the CFR was a factor of ~ 5 lower (assuming a roughly constant rate during this entire period). Based on this observation as our main underlying assumption, we used a simple approach to derive the characteristic cluster disruption time-scale in the LMC, for which we found that $\log(t_4^{\text{dis}} \text{yr}^{-1}) = 9.9 \pm 0.1$, where $t_{\text{dis}} = t_4^{\text{dis}} (M_{\text{cl}}/10^4 M_{\odot})^{0.62}$ (Boutloukos & Lamers 2003; Baumgardt & Makino 2003; Gieles et al. 2005). We argued that this was consistent with earlier, preliminary work done on a smaller cluster sample: Boutloukos & Lamers (2002) found $\log(t_4^{\text{dis}} \text{yr}^{-1}) = 9.7 \pm 0.3$ for a smaller sample of 478 clusters within 5 kpc from the centre of the LMC, in the age range $7.8 \leq \log(\text{age yr}^{-1}) \leq 10.0$. We also considered our result qualitatively consistent with Hunter et al. (2003), who noticed very little destruction of clusters at the high-mass end. This long characteristic disruption time-scale would imply that hardly any of our LMC sample clusters are affected by significant disruptive processes, so that we are in fact observing the *initial* cluster mass function (CMF).

However, a close inspection of fig. 6 of de Grijs & Anders (2006) highlights an apparent contradiction. The “crossing time”, t_{cross} , defined by the crossing point between the best-fitting lines describing the number of clusters per unit time-scale that are mostly affected by fading of their stellar populations and those that are undergoing significant secular disruption, seems to imply that a more appropriate time-scale for the disruption of the LMC cluster system may be of order $\log(t_4^{\text{dis}} \text{yr}^{-1}) \simeq 8.9$. Since this implies a downward adjustment of the characteristic cluster disruption time-scale in the LMC by up to an order of magnitude, we decided to re-investigate the LMC’s cluster disruption history.

Here, we approach this problem from a different angle, by running a large number of Monte-Carlo simulations in which we vary the cluster disruption time-scale. Meanwhile, for each of these cluster disruption time-scales we derive the corresponding CFR required to reproduce the observed cluster age distribution. We then match the observed cluster mass distribution, integrated over time, and the observed two-dimensional distribution of the detected surviving clusters in the $\log(\text{mass})$ vs. $\log(\text{age})$ plane to the model results. χ^2 fit estimates are used to quantify which cluster disruption time-scale and, therefore, which cluster formation history, best describes the presently available data.

This paper is organised as follows. In Section 2 we justify our choices used in the data analysis leading to the cluster age and mass distributions used in the remainder of the paper. Section 3 discusses our basic assumptions in constructing synthetic cluster populations, which we then use in Section 4 to explore the range of characteristic cluster disruption time-scales allowed by the data. In Section 5 we highlight the importance of properly understanding the data’s completeness limit, and use this in Section 6 to constrain possible variations in the CFR over time. In Section 7, we assess precisely what we would need to fully and un-

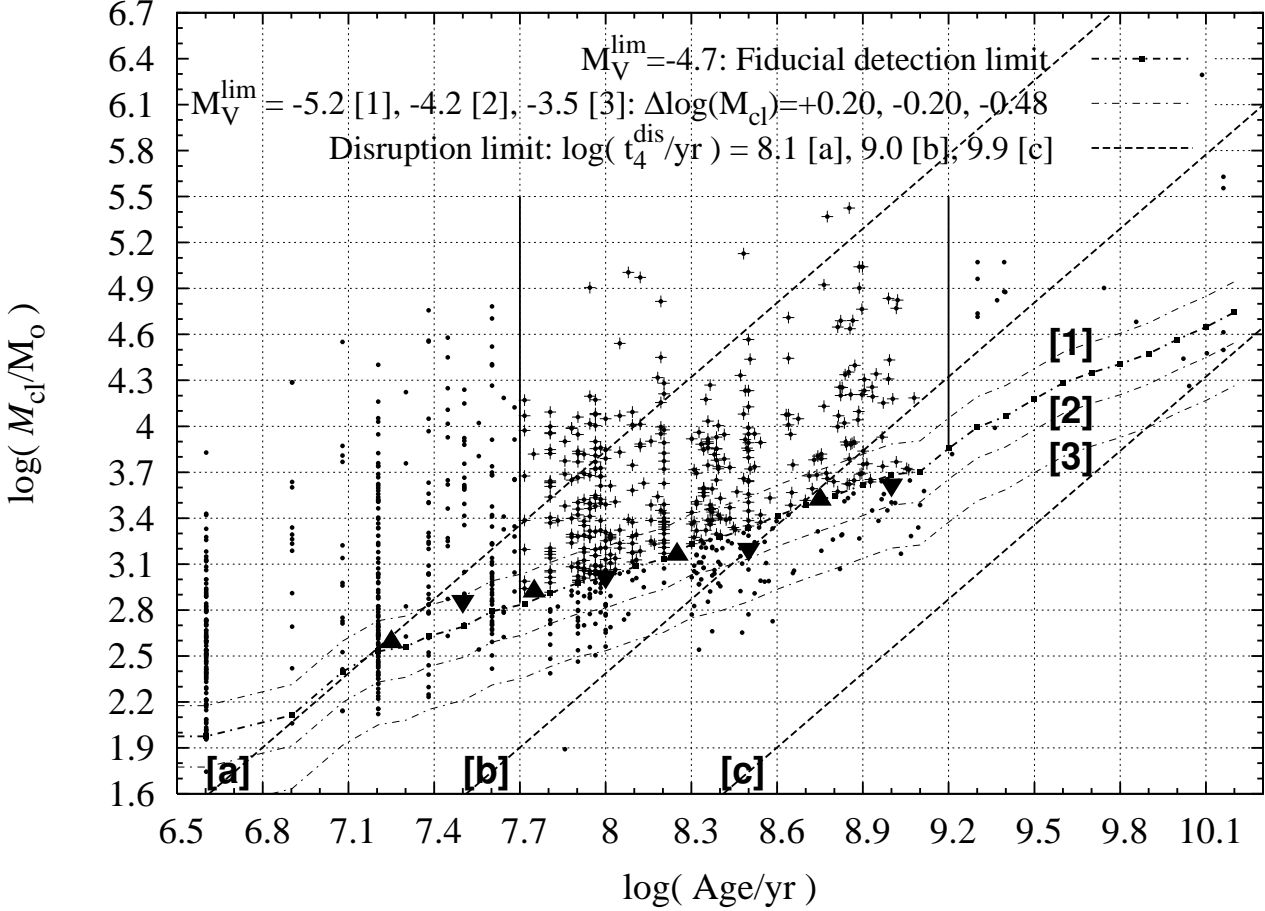


Figure 1. Distribution of the LMC star cluster sample of de Grijs & Anders (2006) in the $[\log(\text{age}), \log(M_{\text{cl}})]$ plane. The filled triangles correspond to the vertical dashed lines in the individual panels of Fig. 2 (upright triangles: left-hand column; upside-down triangles: right-hand column). For subsequent cluster age ranges (in steps of 0.25 dex and 0.5 dex wide) they trace the mass limit below which the sample becomes incomplete (see section 3 for details). They are therefore considered tracers of the fiducial detection limit (thick dash-dotted line with squares), which corresponds to $M_V^{\text{lim}} = -4.7$ mag (based on the GALEV mass-to-light ratios for “simple” stellar populations). The three thin dash-dotted lines, labelled ‘[1]’, ‘[2]’ and ‘[3]’, are the detection limits corresponding to $M_V^{\text{lim}} = -5.2$, $M_V^{\text{lim}} = -4.2$ and $M_V^{\text{lim}} = -3.5$ mag, respectively. They are therefore equivalent to the thick dash-dotted line shifted vertically by, respectively, $\Delta \log(M_{\text{cl}}) = 0.2, -0.2$, and -0.48 . The lower dash-dotted curve (‘[3]’) is the $M_V^{\text{lim}} = -3.5$ mag fading limit of H03. The thick dashed lines represent the cluster disruption limits for $\log(t_4^{\text{dis}} \text{yr}^{-1}) = 8.1, 9.0$ and 9.9 (labelled ‘[a]’, ‘[b]’ and ‘[c]’, respectively). The age range on which we focus in this paper is bracketed by vertical solid lines, at $\log(\text{age yr}^{-1}) = 7.7$ and $\log(\text{age yr}^{-1}) = 9.2$; clusters brighter than $M_V^{\text{lim}} = -4.7$ mag in that age range are represented by crosses

ambiguously constrain t_4^{dis} . Our results and conclusions are summarized in Section 8.

2 DATA

The basis for our detailed re-analysis of the Magellanic Clouds star cluster systems is provided by the *UBVR* broad-band spectral energy distributions (SEDs) of H03, based on Massey’s (2002) CCD survey of the Magellanic Clouds.

In a series of recent papers, we developed a sophisticated tool for star cluster analysis based on broad-band SEDs, ANALYSED, which we tested extensively both internally (de Grijs et al. 2003b,c; Anders et al. 2004) and externally (de Grijs et al. 2005), using both theoretical and observed young to intermediate-age ($\lesssim 3 \times 10^9$ yr) star cluster SEDs, and the GALEV “simple” stellar population (SSP) models (Kurth et

al. 1999; Schulz et al. 2002). The accuracy for younger ages has since been increased via the inclusion of an extensive set of nebular emission lines, as well as gaseous continuum emission (Anders & Fritze-v. Alvensleben 2003). We concluded that the *relative* ages and masses within a given cluster system can be determined to a very high accuracy depending on the specific combination of passbands used (Anders et al. 2004). Even when comparing the results of different groups using the same data set, we can retrieve prominent features in the cluster age and mass distributions to within $\Delta \langle \log(\text{age yr}^{-1}) \rangle \leq 0.35$ and $\Delta \langle \log(M_{\text{cl}}/M_{\odot}) \rangle \leq 0.14$, respectively (de Grijs et al. 2005), which confirms that we understand the uncertainties associated with the use of our ANALYSED tool to a very high degree.

In de Grijs & Anders (2006) we presented newly and homogeneously redetermined age and mass estimates for the entire Large Magellanic Cloud (LMC) star cluster sample

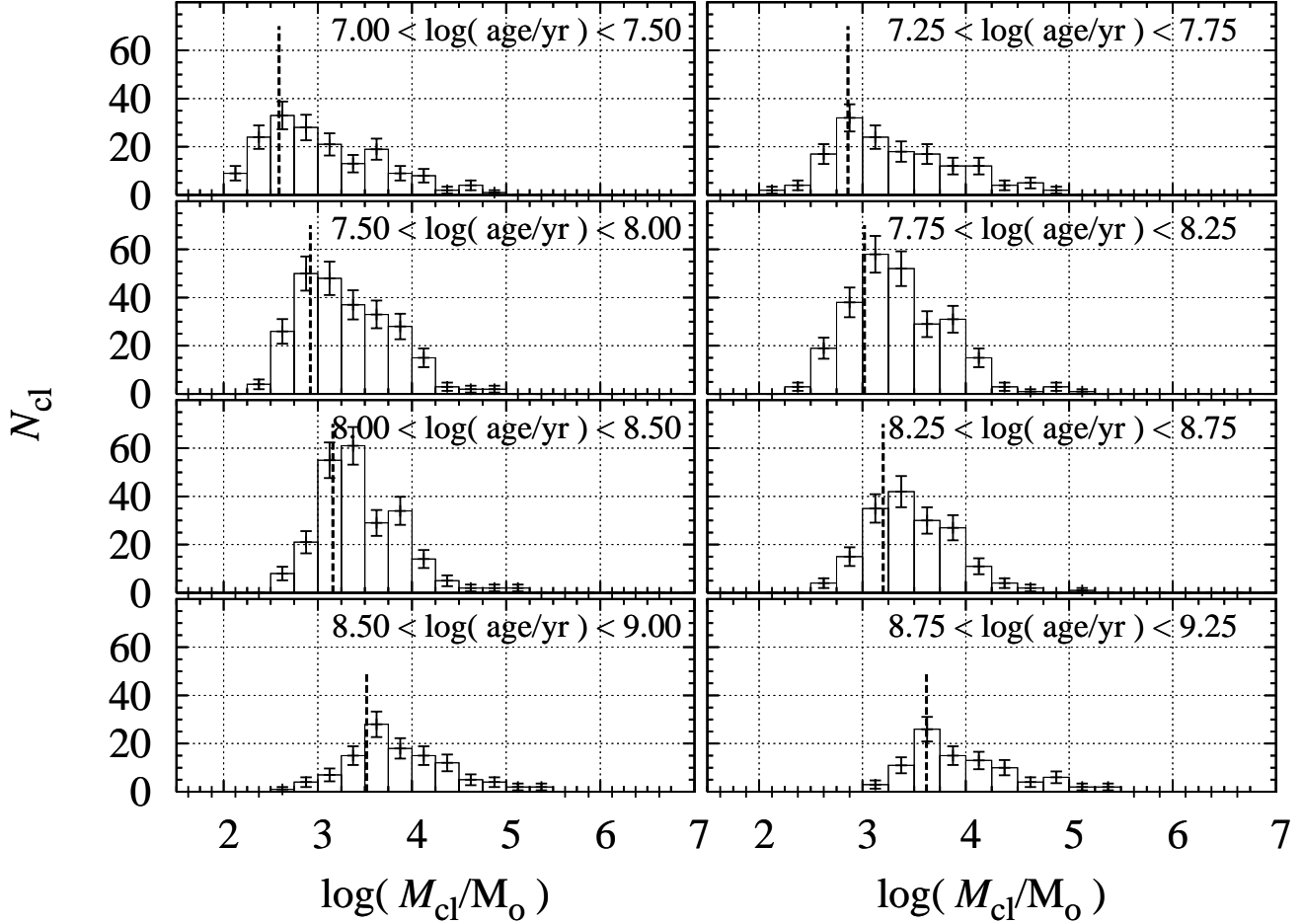


Figure 2. Observed cluster mass functions for the age ranges included at the top of each panel. In each panel, the vertical dashed line is the mass limit bracketing 25 and 75 per cent of the cluster subsample on either side. This is a good proxy to the cluster mass at the turn-over of each CMF. For each age range, turn-over masses are indicated in $(\log(\text{age}), \log(M_{\text{cl}}))$ space as filled triangles in Fig. 1. The mass limits defined by the dashed lines evolve with time following a line of constant luminosity, at $M_V = -4.7$ mag. This implies that the decrease in cluster numbers observed for each CMF below its turn-over mass (i.e. below the vertical dashed line) is mostly driven by incompleteness effects

covered by the Massey (2002) data. Our cluster age and mass determinations assume an average metallicity of $Z = 0.008$ (where $Z_{\odot} = 0.020$); for the total extinction towards the LMC clusters, we assumed $E(B - V) = 0.10$ mag, using the Calzetti attenuation law (Calzetti 1997, 2001; Calzetti et al. 2000; Leitherer et al. 2002) with $R_V = 4.05$. This corresponds to $E(B - V) \simeq 0.13$ mag for both the Cardelli et al. (1989) and the Schlegel et al. (1998) extinction laws. Based on the comparison of our results in de Grijs & Anders (2006) with those published previously in a range of independent studies, and additionally on a detailed assessment of the age-metallicity and age-extinction degeneracies, we concluded that our broad-band SED fits yield reliable ages, with statistical *absolute* uncertainties within $\Delta \log(\text{age yr}^{-1}) \simeq 0.4$ overall.

The determination of the 50 per cent completeness limit of the LMC cluster data was in essence based on a close inspection of H03’s fig. 4. These authors selected their sample from the existing catalogues of Bica et al. (1999) and Pietrzyński et al. (1999), matched to the observational field of view of the Massey (2002) data. Therefore, our completeness is that of these catalogues; Hunter and her team did

not quantify the completeness levels themselves (D. Hunter, priv. comm.), although they discuss an observed fading limit. However, for our analysis it is important to understand the sample incompleteness affecting our observations (although this may not be a strict “limit”, but a “range” instead, given the nature of the LMC cluster sample). As such, we adopted the conservative approach that the present-day LMC cluster luminosity function (CLF; see H03’s fig. 4) is best represented by a power-law function in luminosity. We obtained the best-fitting power law to the LMC’s CLF for $M_V \leq -4.5$ mag, where we assume the cluster sample to be affected by negligible incompleteness. Based on this assumption, we determined the 50 per cent completeness limit to occur at $M_V = -4.25 \pm 0.25$ mag, i.e., at level brighter by about 0.75 mag than H03’s observed fading limit. We note that if the underlying CLF is *not* a power law (e.g., because of fading and secular evolution), the limit we adopt following this approach is in fact a lower limit. In the latter case the observations will likely be more complete than estimated here.

In order to draw statistically robust conclusions from the simulations performed in this paper, knowledge of the

brightness limit M_V^{lim} above which the sample can be considered (fairly) complete is required. In section 3, we will derive an estimate of M_V^{lim} from a close inspection of the evolution with time of the observed CMF.

3 BUILDING SYNTHETIC CLUSTER POPULATIONS ABOVE THE FIDUCIAL DETECTION LIMIT

In order to estimate the characteristic disruption time-scale of the LMC clusters, we set up a grid of synthetic cluster populations governed by various cluster formation histories, ICMFs and disruption time-scales. The age and mass distributions of the surviving clusters brighter than a given detection limit (see below) are then compared to their observational counterparts in order to retrieve the best possible constraints on the formation and evolution history of the LMC star cluster system.

For the ICMF we assume a power-law mass spectrum $dN/dM_{\text{cl}} \propto M_{\text{cl}}^{-2}$ over the mass range $10^2 M_{\odot} - 10^7 M_{\odot}$. Power-law cluster mass spectra with slope $\simeq -2$ have been found for the young cluster systems in the Antennae system (e.g., Zhang & Fall 1999), the Whirlpool galaxy M51 (Bik et al. 2003) and for the Galactic open clusters (Battinelli et al. 1994; Lada & Lada 2003).

Our knowledge of the cluster *formation* history of the LMC remains rather poor at present. In order to explore the LMC's CFR, star clusters are first distributed based on a constant cluster formation rate. For each synthetic cluster population, the age distribution of the surviving clusters that are more massive than the detection limit is compared to that observed. From that comparison, the CFR is corrected in order to match the modelled to the observed age distribution. We will illustrate this step in Section 4. Regarding the cluster age range, the cluster sample we will first be focusing on spans the logarithmic age range $7.7 < \log(\text{age yr}^{-1}) < 9.2$. Since our aim is to estimate the *secular* cluster disruption time-scale, avoiding the first 50 Myr is crucial, as discussed in Section 1. For the upper limit to the age range we adopt $\log(\text{age yr}^{-1}) = 9.2$, since at older ages our cluster sample contains very few objects. Once we have a firm grasp on the cluster formation history for ages $7.7 < \log(\text{age yr}^{-1}) < 9.2$, we will proceed one step further and infer what the cluster formation history at older ages might have been (see Section 6).

Now that we have defined the initial conditions of our fiducial cluster populations in terms of their ages and masses, we have to evolve each cluster mass over time. Lamers et al. (2005b) showed that the decreasing mass of a cluster can be described accurately as:

$$\frac{M_{\text{cl}}(t)}{M_i} = \left\{ \left[\mu_{\text{ev}}(t) \right]^{\gamma} - \frac{\gamma t}{t^{\text{dis}}} \right\}^{1/\gamma}, \quad (1)$$

where $M_{\text{cl}}(t)$ is the mass of a cluster with initial mass M_i that is still bound at an age t . In Eq. 1, $\mu_{\text{ev}}(t)$ is the fractional mass decrease of the cluster because of stellar evolution only. The temporal evolution of $\mu_{\text{ev}}(t)$ is given by eqs. (2) and (3) of Lamers et al. (2005b), which match the predictions of the GALEV “simple” stellar population models very accurately. As for the cluster disruption time-scale t^{dis} ,

it scales with the disruption time-scale t_4^{dis} of a star cluster with an initial mass of $10^4 M_{\odot}$ as

$$t^{\text{dis}} = t_4^{\text{dis}} (M_i / 10^4 M_{\odot})^{\gamma}. \quad (2)$$

With $\gamma = 0.62$, these analytical descriptions of the evolution of the mass of a given cluster matches the results of Baumgardt & Makino (2003), those being based on a large set of N -body simulations, where the combined effects of stellar evolution, two-body relaxation and an external tidal field were taken into account (see also Boutloukos & Lamers 2003 and Gieles et al. 2005 for empirical estimates of γ ; but see also Waters et al. 2006 and section 4 for another γ value). In what follows, the rate of cluster disruption is quantified by the estimate of t_4^{dis} .

Once we have evolved the cluster masses to the appropriate ages based on the adopted CFR sampling, surviving clusters ending up below the detection limit are excluded from the output sample. Because star clusters fade with time as a result of stellar evolution, any magnitude-limited cluster sample will be affected by an increasing lower mass limit with increasing age, thus making it harder to detect low-mass clusters at old age. Figure 1 shows the cluster sample in $\log(\text{mass})$ versus $\log(\text{age})$ space, based on the analysis of de Grijs & Anders (2006). Although the lower cluster mass increases with increasing age as expected, the distribution does not show a *sharp* lower-mass cut-off. This is owing to the nature of the sample, as it is in essence based on published cluster catalogues, each affected by their own sampling characteristics. To establish whether the cluster sample in Fig. 1 is in fact magnitude-limited and, if so, to determine the magnitude limit above which the sample is (fairly) complete, we must therefore resort to empirical means.

Figure 2 shows the cluster mass functions (i.e., the number of clusters per logarithmic cluster mass interval) as a function of age. Specifically, each panel of Fig. 2 displays the mass function of a star cluster subsample covering 0.5 dex in $\log(\text{age})$ in steps of 0.25 dex, as indicated in the panel legends. Each mass function exhibits a turn-over. If this marks the age-dependent lower cluster mass limit below which incompleteness affects the cluster sample significantly, then the turn-over mass as a function of age must follow a trend parallel to the detection limit in the $(\log(\text{age}), \log(M_{\text{cl}}))$ plane (i.e. one of the dash-dotted lines in Fig. 1). For each of the cluster mass functions, the turn-over mass is well-represented by the vertical thick dashed lines in the panels of Fig. 2. This is defined as the mass limit bracketing 25 and 75 per cent of the relevant cluster subsample. The evolution of that mass limit with cluster age is shown as the triangles (upright/upside-down triangles for the left/right-hand panels) in Fig. 1. We note that they follow closely a line of constant magnitude, corresponding to $M_V = -4.7$ mag (thick dash-dotted line with small squares). This result implies that our star cluster sample is predominantly magnitude-limited. The decrease in cluster numbers below the vertical line in each panel of Fig. 2 (i.e., below the turn-over mass) is mostly driven by incompleteness effects, affecting clusters fainter than $M_V = -4.7$ mag. In the following, we adopt $M_V^{\text{lim}} = -4.7$ mag as the magnitude limit above which our sample is reasonably complete, referred to by the “fiducial detection limit”. Comparisons between our model output and the photometric estimates of the cluster ages and masses will be limited to star clusters of $M_V \leq -4.7$

mag. This represents a sample of 375 clusters, identified by crosses in Fig. 1. In section 5, we will investigate how the estimate for the cluster disruption time-scale depends on this mass limit in $(\log(\text{age}), \log(M_{\text{cl}}))$ space.

In summary, we have described how we evolve cluster populations drawn from a given ICMF, and characterised by a given CFR and disruption rate. We have also defined a criterion to separate the surviving clusters of interest from those expected to be affected by significant levels of incompleteness. We are now ready to compare these synthetic populations to the observed cluster sample, represented by the crosses in Fig. 1, in terms of (i) the age distribution, (ii) the mass distribution and (iii) the two-dimensional $(\log(\text{age}), \log(M_{\text{cl}}))$ plane. To do so, both the observed and the model distributions for the clusters in the age range $7.7 < \log(\text{age yr}^{-1}) < 9.2$ and above the detection limit at $M_V^{\text{lim}} = -4.7$ mag are binned identically. We adopt bins of 0.3 dex in both $\log(\text{age})$ and $\log(M_{\text{cl}})$. The corresponding distribution of cells in $(\log(\text{age}), \log(M_{\text{cl}}))$ space is shown as the grid in Fig. 1. In the next section, we will make sure that the choice of the bin size does not affect our results. Given the presence of Poissonian statistics in both the data and the modelling, the goodness-of-fit is quantified using the Poisson Probability Law (*PPL*) introduced by Dolphin (2002) (see also Dolphin & Kennicutt 2002). This follows

$$PPL = 2 \sum_{i=1}^N \left(m_i - n_i + n_i \ln \frac{n_i}{m_i} \right), \quad (3)$$

where N is the number of cells, m_i the predicted number of clusters in cell i and n_i its observed counterpart. The *PPL* estimator is the Poissonian equivalent of the χ^2 estimator, i.e., lower values correspond to a better description of the data. Once divided by the number of bins minus the number of degrees of freedom, we obtain the reduced *PPL*, which we refer to as χ_ν^2 .

4 CLUSTER DISRUPTION TIME-SCALE

As mentioned in Section 1, to infer an estimate (or a range of estimates, as we will see below) for the cluster disruption time-scale is equivalent to deducing the temporal evolution of the LMC's CFR over the past 1.5 Gyr (i.e., up to the upper age limit we consider at the present stage of our analysis).

First, we simulated the evolution of 20 putative star cluster systems. They are all characterized by a constant CFR over the age range $7.7 < \log(\text{age yr}^{-1}) < 9.2$ and have the same power-law ICMF of spectral index $\alpha = -2$. The cluster systems differ with respect to their cluster disruption time-scales, for which twenty values were tested, i.e., $\log(t_4^{\text{dis}} \text{yr}^{-1}) = 8.1$ to 10.0 in steps of 0.1 dex. We then normalise the evolved cluster age/mass distributions so that they contain a constant number of 375 clusters, to match the observations. The initial distributions (e.g., the CFR) follow from this. As a result, a shorter cluster disruption time-scale implies a higher CFR, in order to maintain the present number of observed clusters despite more vigorous disruption. In practice, the CFR for $\log(t_4^{\text{dis}} \text{yr}^{-1}) = 8.1$ is ten times higher than for $\log(t_4^{\text{dis}} \text{yr}^{-1}) = 9.9$ (see top panel of Fig. 3).

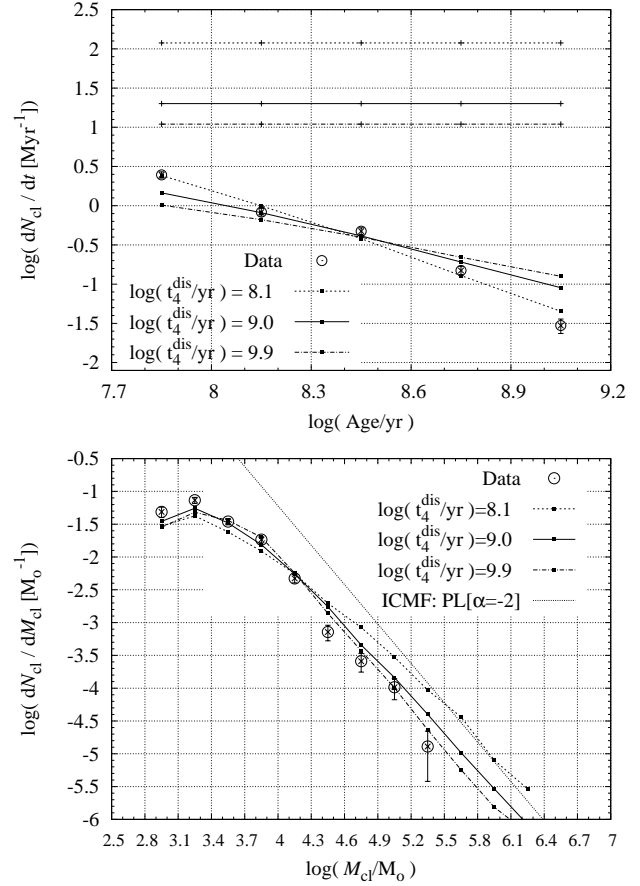


Figure 3. *Top:* Age distribution of the LMC star clusters brighter than the fiducial detection limit at $M_V^{\text{lim}} = -4.7$ mag (i.e. more massive than the thick dash-dotted line in Fig. 1) integrated over mass (large circles with error bars). The lower curves with small squares are their modelled counterparts for three cluster disruption time-scales, $\log(t_4^{\text{dis}} \text{yr}^{-1}) = 8.1, 9.0$ and 9.9 . They have been shifted vertically in order to contain 375 clusters as observed. The upper horizontal straight lines are the corresponding CFRs (assumed constant here). *Bottom:* Same for the evolved cluster mass spectra (i.e., the number of clusters per constant linear mass interval) integrated over age. The dotted straight line shows the slope $\alpha = -2$ of the power-law initial cluster mass spectrum.

When the cluster disruption time-scale is long (e.g., $\log(t_4^{\text{dis}} \text{yr}^{-1}) = 9.9$), the decrease in the number of evolved clusters per time unit as a function of increasing age is dominated by fading effects. The slope of the age distribution therefore mirrors the slope $\zeta \simeq 0.7$ of the lower mass limit over time in $(\log(\text{age}), \log(M_{\text{cl}}))$ space and is $\zeta(1+\alpha) \simeq -0.7$ ($\alpha \simeq -2$). In the opposite case, when the cluster disruption time-scale is short (e.g., $\log(t_4^{\text{dis}} \text{yr}^{-1}) = 8.1$), the slope of the age distribution is mostly determined by disruption and follows $(1-\alpha)/\gamma \simeq -1.6$ (see Boutloukos & Lamers 2003 for an in-depth discussion).

From the observed age distribution alone, one may deduce that the characteristic disruption time-scale of a $10^4 M_\odot$ cluster in the LMC is close to 100 Myr. Shown graphically, in the top panel of Fig. 3, the lower dotted curve (corresponding to the age distribution for $\log(t_4^{\text{dis}} \text{yr}^{-1}) = 8.1$) follows the data points better than the dash-dotted curve (i.e., the age distribution for $\log(t_4^{\text{dis}} \text{yr}^{-1}) = 9.9$). In the lat-

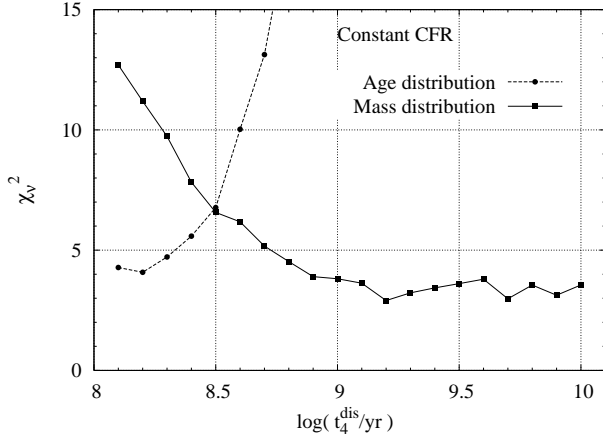


Figure 4. Reduced χ_ν^2 as a function of the characteristic disruption time-scale, t_4^{dis} , of a $10^4 M_\odot$ cluster, as inferred from the age distribution integrated over mass and the mass distribution integrated over age of the detected surviving clusters. Clusters are assumed to have formed with a constant CFR between $\log(\text{age yr}^{-1}) = 7.7$ and $\log(\text{age yr}^{-1}) = 9.2$.

ter case, the predicted age distribution is shallower (with a slope $\simeq -0.7$) than the observed cluster age distribution (exhibiting a slope $\lesssim -1.6$). This conclusion is also supported by the relation between t_4^{dis} and χ_ν^2 for the age distribution (i.e., the long-dashed curve with the filled circles in Fig. 4), which shows a steeply rising χ_ν^2 for $t_4^{\text{dis}} > 200$ Myr.

The $(t_4^{\text{dis}}, \chi_\nu^2)$ relation for the cluster mass spectrum integrated over age paints a completely different picture, however. The short cluster disruption time-scale derived from the age distribution alone now results in a four times larger χ_ν^2 than for $t_4^{\text{dis}} \gtrsim 1$ Gyr (the solid line with filled squares in Fig. 4). The bottom panel of Fig. 3 illustrates that if $\log(t_4^{\text{dis}} \text{yr}^{-1}) = 8.1$, the evolved cluster mass spectrum above $10^4 M_\odot$ is significantly shallower than the observed CMF, of which the slope remains close to that of the ICMF in that mass range. Better fits to the evolved CMF are obtained for $\log(t_4^{\text{dis}} \text{yr}^{-1}) = 9.0$ and 9.9 . This discrepancy between two different estimators for the model goodness-of-fit, χ_ν^2 from the age distribution and χ_ν^2 from the mass distribution, suggests an inconsistent hypothesis, presumably the assumption of a constant CFR.

It is worth emphasising that a possibly variable CFR in the LMC should not be considered as an obstacle to the derivation of the cluster disruption time-scale. Any sufficiently old, coeval subsample of clusters is suitable to infer it, as long as the imprint of the secular dynamical evolution can be detected. In fact, the limited age range of a coeval population ensures that temporal CFR variations can safely be ignored. The imprint of the secular dynamical evolution leads to a turn-over in the CMF. Provided that the shape of the ICMF is known, the disruption time-scale for the relevant environmental conditions can be derived from the combination of the mean cluster age and of the cluster mass at the CMF turn-over (see Section 7 and Fig. 17). This argument is supported by our recent study of the roughly coeval intermediate-age cluster population in M82 B (de Grijs, Parmentier & Lamers 2005; but see also Smith et al. 2007 for updated M82 B data).

In the following, we build on this principle. Specifi-

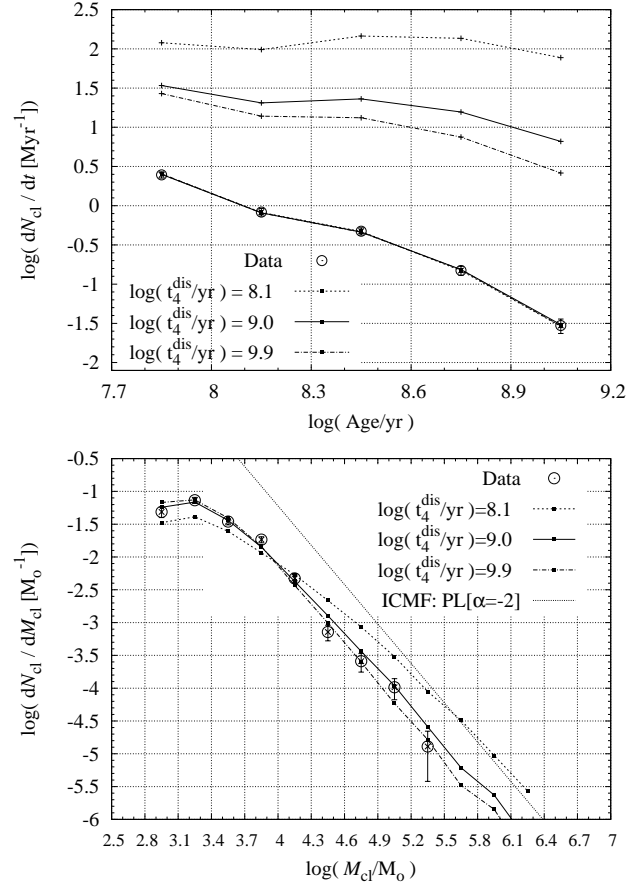


Figure 5. Same as Fig. 3 except for the CFR, which in this case is adjusted in order to match the model age distribution to the observed distribution for each cluster disruption time-scale. *Top:* Cluster age distributions *Bottom:* Cluster mass spectra

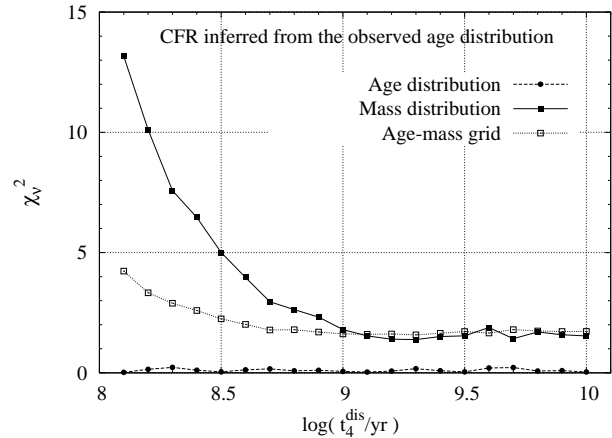


Figure 6. Reduced χ_ν^2 as a function of t_4^{dis} for model cluster age distributions reproducing the observed distribution via CFR adjustments (top panel of Fig. 5). χ_ν^2 functions are shown for the cluster age distribution (equal to zero but for size-of-sample related Poissonian noise), for the cluster mass spectrum and for the two-dimensional distribution of clusters in $(\log(\text{age}), \log(M_{cl}))$ space.

cally, we split the cluster age range under consideration, $7.7 < \log(\text{age yr}^{-1}) < 9.2$, into five subranges, each with a width of $\Delta \log(\text{age yr}^{-1}) = 0.3$ (i.e., the size of a cell in Fig. 1). We assume that these age bins are narrow enough so that each can be characterised by a single CFR. For each of the twenty disruption time-scales explored, we first assume a constant CFR and we derive the corresponding age distribution of the observed survivors. From the comparison between the modelled and the observed age distributions the CFR is adjusted so that the distributions match each other. This is illustrated in the top panel of Fig. 5. Varying the cluster disruption time-scale now leads to distinct cluster formation histories, not only with respect to the mean CFR, but also with respect to its temporal variations. If the cluster disruption time-scale is $\log(t_4^{\text{dis}} \text{yr}^{-1}) = 8.1$, the CFR is almost constant and of order 100 clusters per Myr. This is consistent with what we concluded above (see the top panel of Fig. 3). From that same figure, we also found that if the CFR is constant and if $\log(t_4^{\text{dis}} \text{yr}^{-1}) = 9.0$ or 9.9 , the derived age distribution is shallower than observed. As a result, for such a long cluster disruption time-scale, the LMC cluster age distribution can be matched only by adopting a CFR that decreases with increasing age (compare the top panels of Figs. 3 and 5). Once an appropriate CFR has been adopted for each age bin, the construction of a consistent integrated cluster mass distribution follows naturally (see the bottom panel of Fig. 5).

The relation between the reduced χ_ν^2 and the cluster disruption time-scale t_4^{dis} is presented in Fig. 6. Since the temporal variations in the CFR are adjusted to reproduce the LMC cluster age distribution, the χ_ν^2 for the cluster age distribution is close to zero, regardless of the adopted disruption time-scale. Its best estimate must now be inferred from the χ_ν^2 for the cluster mass spectrum (the solid curve with the filled squares). The best fits are obtained for $\log(t_4^{\text{dis}} \text{yr}^{-1}) \geq 9.0$, for which χ_ν^2 is minimum at $\simeq 1.5$. As for a constant CFR, the shortest tested cluster disruption time-scale ($\log(t_4^{\text{dis}} \text{yr}^{-1}) = 8.1$) leads to an evolved mass spectrum that is significantly shallower than observed (see the short-dashed curve in the bottom panel of Fig. 5).

In Fig. 6, we also show the χ_ν^2 for the distribution of detected clusters in $(\log(\text{age}), \log(M_{\text{cl}}))$ space. The constraints on t_4^{dis} derived from the two-dimensional distribution of data points are significantly looser than those obtained from the mass spectrum (see Table 1). This likely results from the smaller number of clusters in each grid cell than in the mass distribution bins, leading to larger error bars and hence more poorly determined constraints (see also Section 7). From the results shown in Fig. 6, we conclude that the best constraint we can set on the characteristic cluster disruption time-scale in the LMC is $t_4^{\text{dis}} \geq 1$ Gyr. As we will discuss in Section 7, the presently available data do not allow us to distinguish between $t_4^{\text{dis}} = 1$ and 10 Gyr.

Table 1 lists the cluster disruption time-scales (or a range of cluster disruption time-scales where relevant) corresponding to the minimum χ_ν^2 for the cases discussed in this section, as well as those presented in Section 5. Also given is the range of accepted cluster disruption time-scales defined as the most extreme models which satisfy $\chi_\nu^2 \leq \chi_{\nu, \text{min}}^2 + 1$.

We now test how robust the χ_ν^2 functions are with respect to our input parameters. Fig. 7 shows that they remain practically unaffected when the adopted ICMF upper limit

Table 1. Summary of the various Poissonian χ^2 tests. The first column describes the diagnostic used to compare the model to the data, either the mass function or the age-mass grid. For the fiducial case, we also include the results for each of the five mass functions per age bin, with each age range quoted as $[\min(\log(\text{age yr}^{-1})), \text{Max}(\log(\text{age yr}^{-1}))]$. The second column tabulates the minimum χ_ν^2 . The third column contains, first, $\log(t_4^{\text{dis}} \text{yr}^{-1})$ at which χ_ν^2 is minimum, and secondly the range of $\log(t_4^{\text{dis}} \text{yr}^{-1})$ for which $\chi_\nu^2 \leq \chi_{\nu, \text{min}}^2 + 1$. The fourth column refers to the relevant figure. Results are provided for the fiducial case, for other detection limits corresponding to the three thin dash-dotted lines in Fig. 1 (referred to by the amplitude of the vertical shift in $\log(M_{\text{cl}})$ with respect to the fiducial detection limit; see section 5), for ICMFs with different slopes ($\alpha = -1.9$ and -2.1) and for a different model of cluster mass-loss ($\gamma = 1$ in equations 1 and 2).

	$\chi_{\nu, \text{min}}^2$	$\log(t_4^{\text{dis}} \text{yr}^{-1})$	
Fiducial Case			
Mass function	$\simeq 1.5$	$(\geq 9.10, \geq 8.85)$	Fig. 6
Age-mass grid	$\simeq 1.7$	$(\geq 8.70, \geq 8.35)$	Fig. 6
CMF [7.7-8.0]	$\simeq 2.5$	$(8.70, \text{any})$	Fig. 8
CMF [8.0-8.3]	$\simeq 1.3$	$(\geq 9.00, \geq 8.55)$	Fig. 8
CMF [8.3-8.6]	$\simeq 2.0$	$(\geq 9.40, \geq 9.0)$	Fig. 8
CMF [8.6-8.9]	$\simeq 0.9$	$(9.00, [8.5, 9.7])$	Fig. 8
CMF [8.9-9.2]	$\simeq 0.8$	$(\geq 9.2, \geq 8.7)$	Fig. 8
$\alpha = -1.9$			
Mass function	$\simeq 1.7$	$(\geq 9.40, \geq 9.00)$	Fig. 7
Age-mass grid	$\simeq 1.6$	$(\geq 8.90, \geq 8.45)$	Fig. 7
$\alpha = -2.1$			
Mass function	$\simeq 1.4$	$(\simeq 9.30, \geq 8.65)$	Fig. 7
Age-mass grid	$\simeq 1.6$	$(\simeq 8.80, \geq 8.25)$	Fig. 7
$\gamma = 1.00$			
Mass function	$\simeq 1.4$	$(\geq 9.20, \geq 9.05)$	Fig. 7
Age-mass grid	$\simeq 1.7$	$(\geq 8.90, \geq 8.60)$	Fig. 7
$\Delta \log(M_{\text{cl}}) = +0.20$ (line ‘[1]’ in Fig. 1)			
Mass function	$\simeq 1.6$	$(\geq 9.10, \geq 8.70)$	Fig. 12
Age-mass grid	$\simeq 2.0$	$(\geq 8.70, \geq 8.45)$	Fig. 12
$\Delta \log(M_{\text{cl}}) = -0.20$ (line ‘[2]’ in Fig. 1)			
Mass function	$\simeq 3.0$	$(\simeq 9.00, [8.70, 9.50])$	Fig. 12
Age-mass grid	$\simeq 2.0$	$(\geq 9.00, \geq 8.45)$	Fig. 12
$\Delta \log(M_{\text{cl}}) = -0.48$ (line ‘[3]’ in Fig. 1)			
Mass function	$\simeq 8.4$	$(\geq 8.65, [8.45, 8.90])$	Fig. 12
Age-mass grid	$\simeq 3.1$	$(\geq 8.60, [8.35, 9.30])$	Fig. 12

is lowered from $M_{\text{cl,up}} = 10^7 M_\odot$ down to $M_{\text{cl,up}} = 10^6 M_\odot$ (panel (a)), when the grid in $(\log(\text{age}), \log(M_{\text{cl}}))$ space is shifted by -0.15 dex in both $\log(\text{age})$ and $\log(M_{\text{cl}})$ (panel (d)) and when the size of the grid cells is $\Delta \log(M_{\text{cl}}) = 0.4$ and $\Delta \log(\text{age}) = 0.4$ dex (instead of 0.3 dex, panel (e)). In all panels, these three cases are illustrated by the thick curves, along with thin curves representing the fiducial case (from Fig. 6). The t_4^{dis} ranges over which χ_ν^2 is minimum is practically the same as for the fiducial case. Our conclusions thus prove robust with respect to these variations.

Thus far, we have assumed a power-law initial cluster mass spectrum with a slope of $\alpha = -2$ for our synthetic

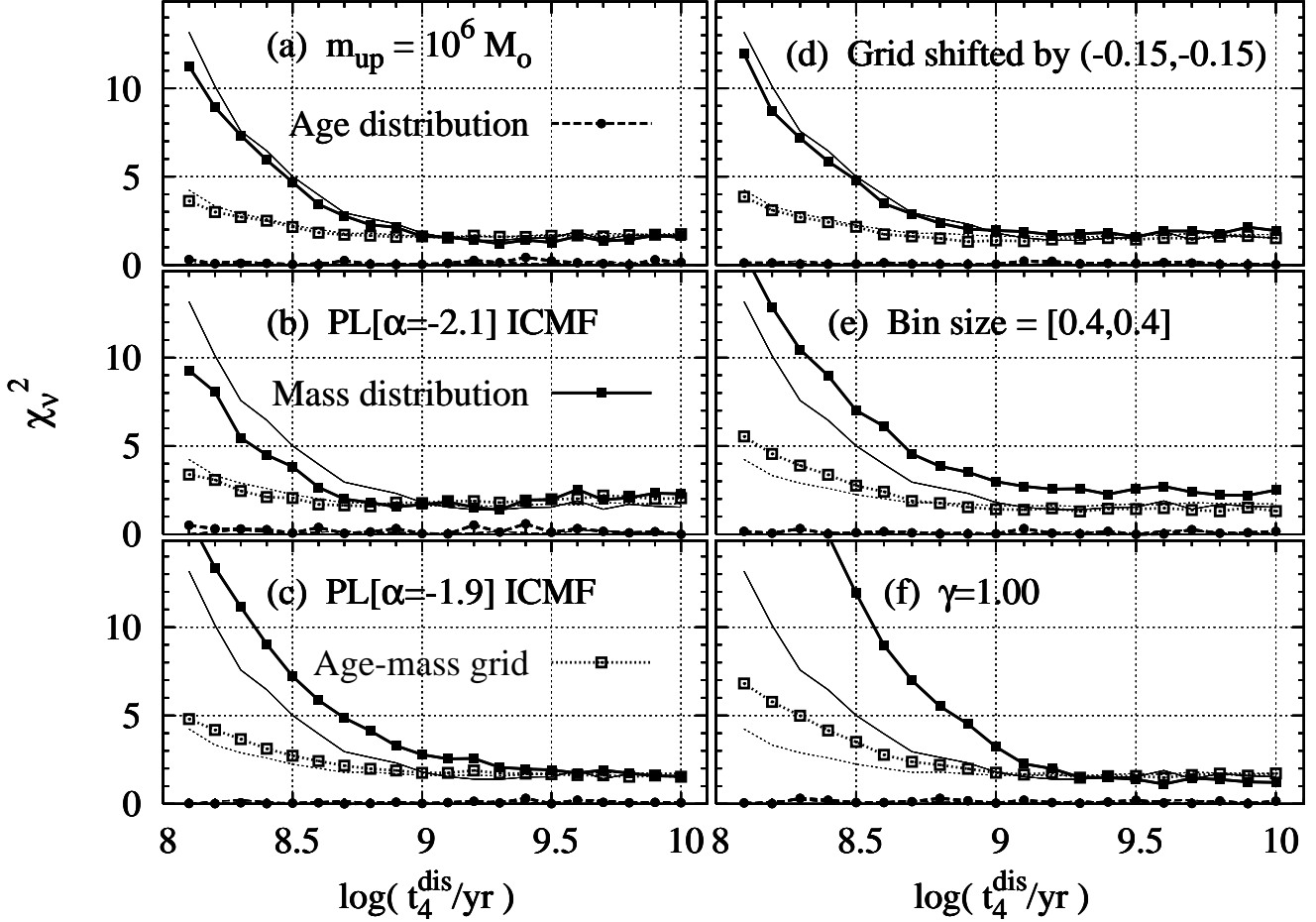


Figure 7. Evolution of the reduced χ_ν^2 vs. cluster disruption time-scale t_4^{dis} for seven different models applied to the data. The fiducial case (upper limit of the cluster mass distribution $M_{\text{cl,up}} = 10^7 M_\odot$, ICMF spectral index $\alpha = -2$, grid location and cell size as shown in Fig. 1, $\gamma = 0.62$) is shown as the thin symbol-free lines in each panel for the sake of comparison. The subsequent panels consider: (a) a different upper mass limit of $M_{\text{cl,up}} = 10^6 M_\odot$, (b) a steeper power-law ICMF with $\alpha = -2.1$, (c) a shallower power-law ICMF with $\alpha = -1.9$, (d) a grid location shifted by -0.15 dex in both $\log(\text{age})$ and $\log(M_{\text{cl}})$, (e) a grid cell size of $\Delta \log(M_{\text{cl}}) = 0.4$ and $\Delta \log(\text{age}) = 0.4$ (instead of 0.3 in the fiducial case), and (f) a larger value of the exponent γ describing the dependence of the disruption timescale on the initial cluster mass (see equations 1 and 2), respectively. The corresponding χ_ν^2 functions are shown as the thick lines with symbols

star cluster systems. Slightly shallower or steeper power laws have been reported in the literature for observed CMFs, however, with $-2.1 \lesssim \alpha \lesssim -1.8$ (see de Grijs et al. 2003c for a review). In panels (b) and (c) of Figure 7, we substituted the canonical ICMF with $\alpha = -2$ by a steeper power law of slope $\alpha = -2.1$ and a shallower power law of slope $\alpha = -1.9$, respectively. A steeper/shallower power law leads to larger/smaller ranges of acceptable t_4^{dis} , although changes are not significant (see also Table 1). Therefore, we conclude that our estimate of the characteristic cluster disruption time-scale in the LMC is also robust with respect to changes in the ICMF, provided that this remains consistent with the observed mass function of bound clusters at young age.

While Boutloukos & Lamers (2003) and Gieles et al. (2005) advocate that the cluster disruption timescale goes as the cluster mass to the power $\gamma = 0.62$, Fall & Zhang (2001) come up with $\gamma = 1$ (see equations 1 and 2). Moreover, in a recent study of the M87 globular cluster system, Waters et al. (2006) find that a cluster evaporation model

with $\gamma = 1$ provides a better match to the observed cluster mass function than if $\gamma = 0.62$ (see also the discussion in Gieles 2007). We thus now assess how much the uncertainties affecting γ propagate as uncertainties on t_4^{dis} . The bottom-right panel of Fig. 7 (panel (f)) compares between $\gamma = 1$ (thick curves) and $\gamma = 0.62$ (fiducial case; thin curves). A greater value of γ sets tighter constraints on the cluster disruption timescale in the sense that the solution $t_4^{\text{dis}} \leq 1$ Gyr is significantly more rejected. A larger γ actually leads to shallower cluster disruption limits in $\log(\text{mass})$ versus $\log(\text{age})$ space (thick dashed lines in Fig. 1). That is, for a fixed value of t_4^{dis} , clusters initially more/less massive than $10^4 M_\odot$ dissolve more slowly/quickly if $\gamma = 1$ than if $\gamma = 0.62$. Owing to the combination of the adopted age range with the fiducial detection limit, clusters less massive than $10^4 M_\odot$ dominate the cluster sample in terms of number. As a result, $\gamma = 1$ mimics a quicker evolutionary rate for the overall cluster population (even though t_4^{dis} is kept unchanged). Therefore, to account either for the *given* observed cluster mass distribution or for the *given* cluster

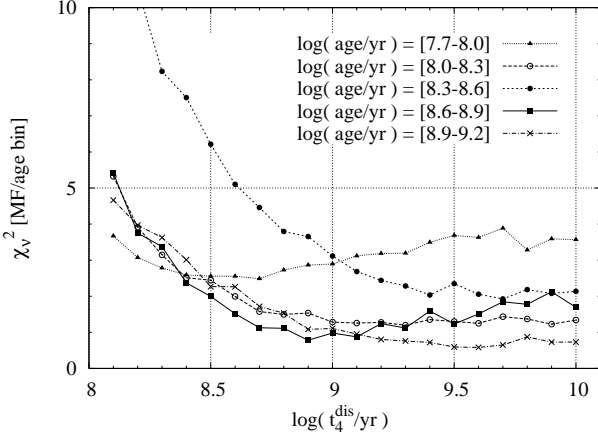


Figure 8. Evolution of χ^2_ν with cluster disruption time-scale t_4^{dis} for the CMFs for each age bin of the fiducial case. The age ranges are listed in the figure legend; they correspond to the age binning used in Fig. 1

sample in $(\log(\text{age}), \log(M_{\text{cl}}))$ space requires a slower cluster disruption timescale when $\gamma = 1$, as illustrated by panel (f) in Fig. 7. The overall conclusions drawn on the basis of the fiducial case, i.e. $t_4^{\text{dis}} \gtrsim 1$ Gyr and temporal variations of the CFR as shown on top panel of Fig. 5, are not affected, however (see also Table 1).

How the χ^2_ν functions depend on variations in the location of the detection limit in $(\log(\text{age}), \log(M_{\text{cl}}))$ space will be discussed in Section 5.

As a way of inspecting more closely the goodness-of-fit of the modelled grid to the data grid, we consider (in Fig. 8) the χ^2_ν functions for each CMF for each age bin. These are listed in the figure legend. All cluster age ranges, except for the first one, support the same conclusion, i.e., $t_4^{\text{dis}} \gtrsim 1$ Gyr (details are provided in Table 1). The tightest constraint is provided by the CMF in the age range $8.3 < \log(\text{age yr}^{-1}) < 8.6$ (χ^2_ν is minimum over the more limited age range $\log(t_4^{\text{dis}} \text{yr}^{-1}) \geq 9.4$), which is also one of the two most populated age bins.

The χ^2_ν function for the age range $7.7 < \log(\text{age yr}^{-1}) < 8.0$ (i.e., the youngest age bin) appears different. At such a young age, the CMF bears the imprint of dynamical evolution only if this proceeds on a short time-scale (e.g., $\log(t_4^{\text{dis}} \text{yr}^{-1}) \simeq 8.1$), which is not the case here. We therefore expect a χ^2_ν function that is flat over most of the disruption time-scale range, except for a possible rise for the very short-time-scales. Actually, the χ^2_ν function is roughly constant over the two-decade t_4^{dis} variations.

In order to carefully represent the cluster distribution in the two-dimensional $(\log(\text{age}), \log(M_{\text{cl}}))$ space, Figs. 9 and 10 show the CMFs per age bin and the cluster age distributions per mass bin, respectively. Model and observed distributions are shown by lines and large open circles, respectively. Note that 1σ error bars are often smaller than the symbol size. The increase with increasing age of the lower mass limit to the CMF (Fig. 9) and the age range extension for greater cluster mass (Fig. 10) mirror the detection limit in $(\log(\text{age}), \log(M_{\text{cl}}))$ space.

As was concluded based on the top panel of Fig. 5,

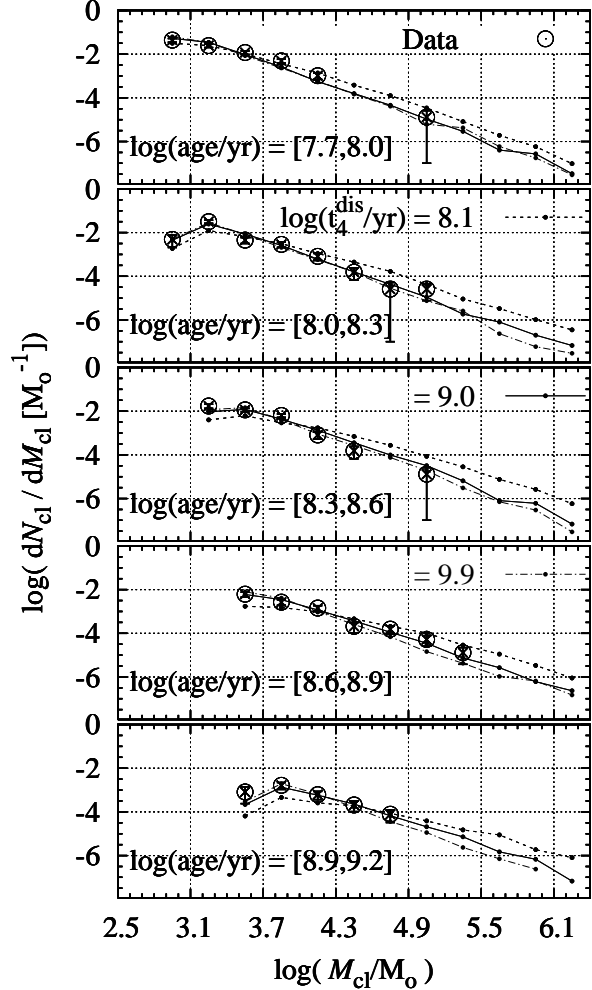


Figure 9. Mass spectra of the detected surviving clusters for the data (large open circles with error bars) and the models (short-dashed lines: $\log(t_4^{\text{dis}} \text{yr}^{-1}) = 8.1$; solid lines: $\log(t_4^{\text{dis}} \text{yr}^{-1}) = 9.0$; dash-dotted lines: $\log(t_4^{\text{dis}} \text{yr}^{-1}) = 9.9$) for the age ranges considered in Fig. 8. They correspond to the age binning used in Fig. 1

should the LMC be characterised by a short cluster disruption time-scale of $\log(t_4^{\text{dis}} \text{yr}^{-1}) = 8.1$, its CFR would also have been higher by a factor of $\simeq 5(10)$ compared to $\log(t_4^{\text{dis}} \text{yr}^{-1}) = 9.0(9.9)$ (see the top panels of Fig. 3 and of Fig. 5). Because massive star clusters dissolve on a longer time-scale than their low-mass counterparts, their age distribution retains a better imprint of the CFR. The two lower right-hand panels in Fig. 10 [$\log(M_{\text{cl}}/M_\odot) > 4.6$] thus show model age distributions in excess of what is observed if $\log(t_4^{\text{dis}} \text{yr}^{-1}) = 8.1$ (short dashed line). On the other hand, in the low-mass regime (say, for $M_{\text{cl}} < 10^4 M_\odot$), where disruption proceeds on a shorter time-scale, the synthetic age distributions are under-represented with respect to the observations (left panels in Fig. 10). Therefore, a cluster disruption time-scale of order $\log(t_4^{\text{dis}} \text{yr}^{-1}) = 8.1$ is ruled out in the LMC since it would give rise to number counts in the cluster age distributions that are lower (higher) than the observations for $\log(M_{\text{cl}}/M_\odot) < 4.0$ (> 4.6), despite the fact that the overall synthetic cluster age distribution, i.e.

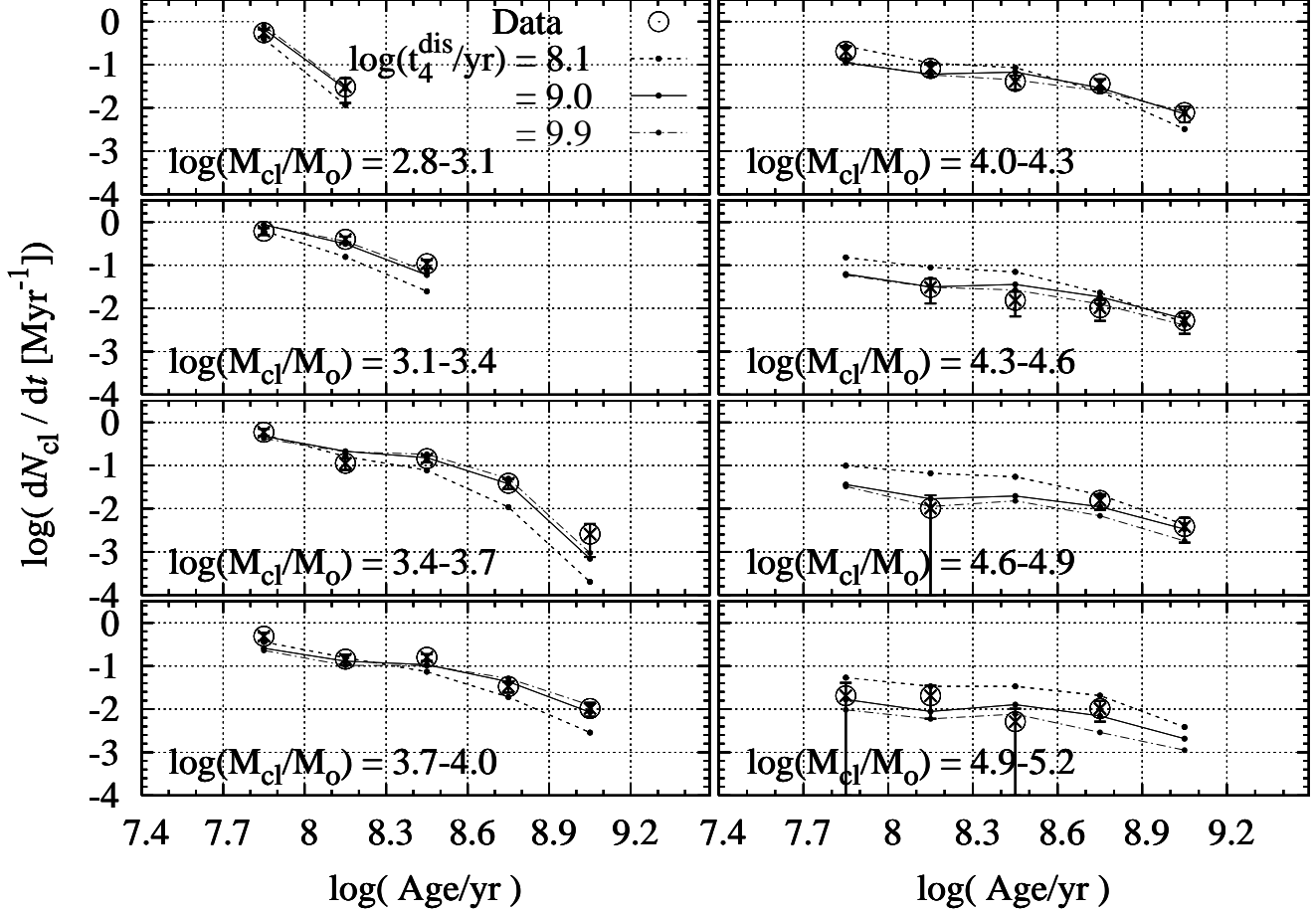


Figure 10. Age distributions of the detected surviving clusters for the data (large open circles with error bars) and the models (short-dashed lines: $\log(t_4^{\text{dis}}/\text{yr}) = 8.1$; solid lines: $\log(t_4^{\text{dis}}/\text{yr}) = 9.0$; dash-dotted lines: $\log(t_4^{\text{dis}}/\text{yr}) = 9.9$) for the eight mass ranges listed at the bottom-left of each panel. They correspond to the mass binning used in Fig. 1

integrated over all cluster masses, matches the observations fairly well.

In order to complete our analysis, we list in Table 2 the ratio F_M between the final total mass and the initial total mass in clusters, and the corresponding number count ratio, F_N (i.e. the fraction of surviving clusters), for the three cluster disruption time-scales considered here and for the case where we adjusted the CFR to match the observed age distribution. We consider the age ranges $7.7 < \log(\text{age yr}^{-1}) < 9.2$ (first part of the table) and $7.7 < \log(\text{age yr}^{-1}) < 10.2$ (second part of the table; see section 6). F_N and F_M refer to the survival rates of all clusters, regardless of their final mass. F_M^{obs} and F_N^{obs} are the survival rates of the *detected* clusters, i.e., those brighter than the adopted detection limit at $M_V^{\text{lim}} = -4.7$ mag. As also found in previous studies (Baumgardt 1998; McLaughlin 1999; Parmentier & Gilmore 2005), number-related quantities are more sensitive to dynamical evolution than mass-related quantities. This is so because, for a power-law ICMF with a spectral index of $\alpha = -2$, low-mass clusters dominate the initial cluster population in terms of number, but not in terms of mass, while they are expected to be disrupted first. For instance, the low-mass range $2 < \log(M_{\text{cl}}/M_{\odot}) < 3$ accounts for only 20 per cent of the total initial mass in clusters (assuming $\alpha = -2$

and a mass range $10^2 < M_{\text{cl}}/M_{\odot} < 10^7$), while their number fraction amounts to about 90 per cent. Finally, we remind the reader that these survival rates do not take into account infant mortality.

5 IMPORTANCE OF A PROPERLY DEFINED DETECTION LIMIT

In this section, we investigate how the estimated range of the LMC's t_4^{dis} responds to vertically shifting the adopted detection limit in Fig. 1. As an extreme case, let us for instance consider H03's fading limit at $M_V = -3.5$ mag as our detection limit (dash-dotted line labelled '[3]' in Fig. 1). The turn-over caused by incompleteness effects in each CMF, for each age bin, would in this case incorrectly be considered as resulting from dynamical evolution. Assuming a power-law ICMF of spectral index $\alpha = -2$, the cluster disruption time-scale can directly be derived from the turn-over cluster mass for each of the cluster age ranges considered. The results of this exercise are shown in Fig. 11. The conclusions from the individual age bins are in conflict with each other. If we consider the oldest age bin ($8.9 < \log(\text{age yr}^{-1}) < 9.2$) only, the range of acceptable values is $9.0 \lesssim \log(t_4^{\text{dis}}/\text{yr}) \lesssim 9.8$. However, in the youngest age bin ($7.7 < \log(\text{age yr}^{-1}) < 8.0$),

Table 2. Cluster survival rates in terms of number counts and in terms of mass. F_N is the ratio between the number of surviving clusters and the initial number of clusters; F_N^{obs} is the ratio between the number of *detected* surviving clusters and the initial number of clusters. F_M and F_M^{obs} are the corresponding quantities in units of cluster mass. These figures are based on a power-law ICMF with a spectral index of $\alpha = -2$, a detection limit at $M_V^{\text{lim}} = -4.7$ mag, and a CFR adjusted so that the modelled age distribution matches the observed LMC cluster age distribution. Survival rates are given for three different cluster disruption time-scales and for two different cluster age ranges.

$\log(t_4^{\text{dis}} \text{yr}^{-1})$	(F_N, F_N^{obs})	(F_M, F_M^{obs})
$7.7 < \log(\text{age yr}^{-1}) < 9.2$		
8.1	$(4 \times 10^{-3}, 2 \times 10^{-3})$	(0.20, 0.20)
9.0	(0.09, 0.02)	(0.47, 0.44)
9.9	(0.49, 0.04)	(0.68, 0.54)
$7.7 < \log(\text{age yr}^{-1}) < 10.2$		
8.1	$(5 \times 10^{-4}, 3 \times 10^{-4})$	(0.03, 0.03)
9.0	(0.03, 0.01)	(0.25, 0.23)
9.9	(0.32, 0.02)	(0.54, 0.43)

there is a turn-over at a cluster mass of about $10^3 M_\odot$ (see Fig. 2, although the age ranges are not strictly identical to those considered in Fig. 11), which would not be expected as owing to dynamical evolution if the cluster disruption time-scale derived from the oldest age range were correct. Consideration of the youngest age bin only therefore results in a cluster disruption time-scale estimate of about $\log(t_4^{\text{dis}} \text{yr}^{-1}) = 8.1 - 8.2$ (see Fig. 11), i.e. a significantly shorter cluster disruption time-scale than found for the oldest age bin. Intermediate values for the cluster disruption time-scale are derived from consideration of the three intermediate age bins.

On a global scale, both the χ_ν^2 obtained from the cluster mass spectrum integrated over age and the χ_ν^2 from the distribution of clusters in $(\log(\text{age}), \log(M_{\text{cl}}))$ space lead to significantly shorter cluster disruption time-scale estimates than what we inferred from the fiducial case. This is shown by the thick curves with filled symbols in the bottom panel of Fig. 12, where we also show the results for the fiducial case (thin curves). Not only does the reduced χ_ν^2 derived from the mass spectrum suggest a shorter $\log(t_4^{\text{dis}} \text{yr}^{-1}) \simeq 8.6 - 8.7$, it also increases significantly for longer cluster disruption time-scales, thus making those longer time-scales less probable (see Table 1). Additionally, its absolute value is high, $\chi_{\nu, \text{min}}^2 \simeq 8$, indicating a poor match between the model and the data.

Lacking a robustly established detection limit, one cannot, therefore, derive a reliable estimate of the cluster disruption time-scale. There is, in fact, a degeneracy between the incompleteness effects and the effects of dynamical evolution, in the sense that the impact of an underestimated completeness limit is mimicked by a shortened disruption time-scale.

The top panels of Fig. 12 show how χ_ν^2 responds to vertical shifts of the fiducial detection limit (i.e. $M_V^{\text{lim}} = -4.7$) by $\Delta \log M_{\text{cl}} = +0.2$ or -0.2 dex (equivalent to ± 0.5 mag; see the dash-dotted lines labelled ‘[1]’ and ‘[2]’ in Fig. 1). In

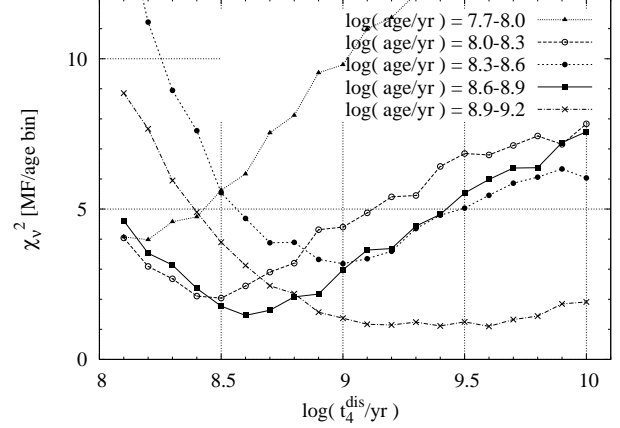


Figure 11. Same as Fig. 8, but assuming a fiducial detection limit decreased by $\Delta \log(M_{\text{cl}}) = -0.48$ dex in $(\log(\text{age}), \log(M_{\text{cl}}))$ space (i.e., to H03’s fading limit). The minima of the χ_ν^2 functions for the various CMFs for given age ranges are located at markedly different cluster disruption time-scales. The inconsistency suggests a problem in the data, namely, the incorrectly estimated detection limit. That is, CMF turn-overs created as a result of incompleteness are interpreted in terms of rapid secular evolution, especially at young ages.

the first case (top panel), they do not differ significantly from the fiducial case except for a loss of sensitivity of the mass spectrum-based χ_ν^2 in the short cluster disruption time-scale regime (i.e., these are less significantly rejected). In the second case (middle panel), the shapes of the χ_ν^2 functions at $\log(t_4^{\text{dis}} \text{yr}^{-1}) < 9.0$ do not differ from the fiducial case. However, longer cluster disruption time-scales are less probable, which illustrates the incompleteness-disruption rate degeneracy referred to above.

6 THE DEPTH OF THE AGE GAP

In the previous section, we have put the best possible constraints on the cluster disruption time-scale based on the distribution of the detected surviving clusters in the most populated part of the $(\log(\text{age}), \log(M_{\text{cl}}))$ diagram. We now take one step further, and infer how the LMC’s CFR may have varied over the past Hubble time. Fig. 13 is the equivalent of the top panel of Fig. 5, but extended up to an age of about 16 Gyr (i.e. the maximum cluster age in the GALEV library). As before, the CFR, adjusted to match the observed age distribution, is shown for the disruption time-scales, $\log(t_4^{\text{dis}} \text{yr}^{-1}) = 8.1, 9.0$, and 9.9 . The slight scatter in the evolved age distributions around the data points is entirely caused by sampling noise, because we limited the number of input clusters to 10^7 for $\log(t_4^{\text{dis}} \text{yr}^{-1}) = 8.1$ and to 4×10^5 for $\log(t_4^{\text{dis}} \text{yr}^{-1}) = 9.9$. This results in a detected survivor census of a few $\times 10^3$ clusters.

Let us now consider the extreme values of our best estimate for the range of cluster disruption time-scales, i.e. $\log(t_4^{\text{dis}} \text{yr}^{-1}) = 9.0$ and 9.9 . The corresponding evolution of the CFR is very similar in both cases. From the epoch of the formation of the first clusters, their number decreases with time, reaching a minimum about 5 Gyr ago, before steadily increasing again and remaining roughly constant for the

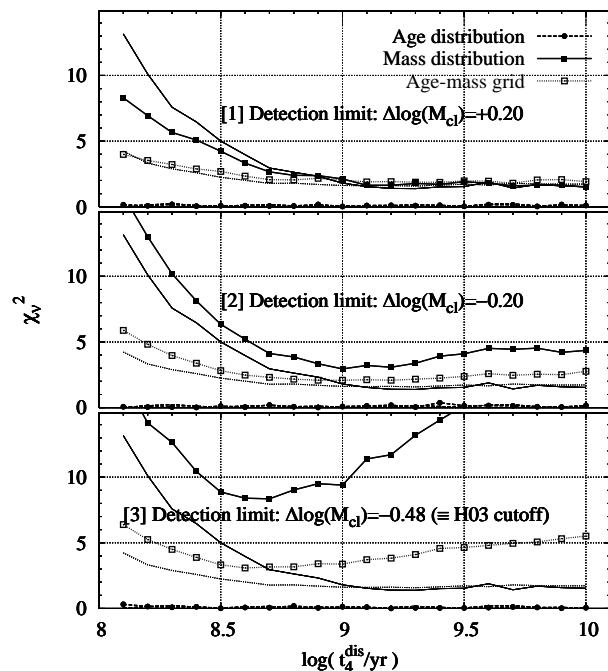


Figure 12. Evolution of χ^2_ν as a function of cluster disruption time-scale, assuming four different detection limits. For comparison, each panel displays the fiducial case as thin lines. The top, middle and bottom panels show the results for detection limits shifted with respect to the fiducial limit by $\Delta \log(M_{cl}) = +0.20, -0.20$, and -0.48 , respectively (corresponding to thin dash-dotted lines labelled ‘[1]’, ‘[2]’ and ‘[3]’ in Fig. 1). The corresponding χ^2_ν values are shown as thick lines with symbols.

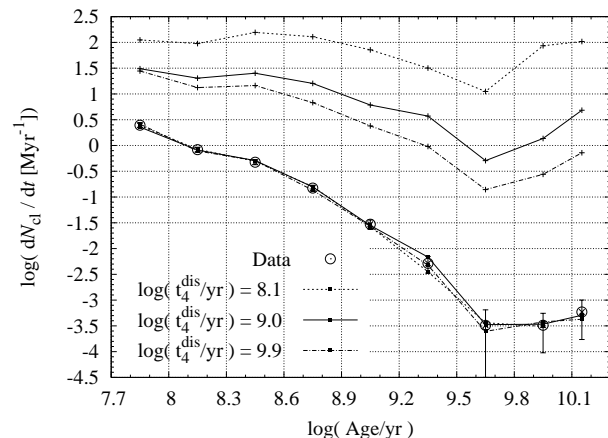


Figure 13. Same as the top panel of Fig. 5, except that the age range has been extended up to 16 Gyr. Note that this figure excludes the age range dominated by infant mortality and infant weight-loss, i.e., the first 50 Myr. The ICMF is assumed to be a power law of spectral index $\alpha = -2$, irrespective of when clusters are formed.

past 300 Myr. The present-day formation rate of the *bound* clusters in the LMC is 30 Myr^{-1} , regardless of whether $\log(t_4^{\text{dis}} \text{ yr}^{-1}) = 9.0$ or 9.9 . At older ages, however, both inferred CFRs differ by a factor of 5 (5 Gyr ago) up to a factor of 8 ($\simeq 10$ Gyr ago). As for the 5 Gyr-old “CFR gap” (mirroring the presently observed cluster age gap, but see below),

this is characterised by a CFR of 30 (for $\log(t_4^{\text{dis}} \text{ yr}^{-1}) = 9.0$) to 100 (for $\log(t_4^{\text{dis}} \text{ yr}^{-1}) = 9.9$) times lower than its present-day value.

Previous estimates of the depth of the age gap had already been provided by H03 and de Grijs & Anders (2006). From the temporal evolution of the maximum cluster mass, and assuming that the mass of the most massive cluster is determined by size-of-sample effects, H03 infers that the CFR has approximately varied with age as $\text{CFR} \propto \text{age}^{-1}$ between 100 Myr and 10 Gyr ago (their fig. 8). This implies that 5 Gyr ago, the CFR was ~ 50 times lower than 100 Myr ago, which matches our own estimates above quite well. As H03 cautions, however, their result heavily depends on the age and mass estimates of the few clusters in the age gap.

From the cluster age distribution of de Grijs & Anders (2006, their fig. 6a), we derive a seemingly more limited CFR variation. The vertical shift between the observed age distribution and the age distribution predicted for a constant CFR (i.e., their disruption line) at an age of 5 Gyr shows an equivalent ratio of ~ 10 only. Since their $\log(t_{\text{cross}} \text{ yr}^{-1}) \simeq 8.1$ implies $t_4^{\text{dis}} \simeq 1$ Gyr, only the comparison to our CFR ratio for $\log(t_4^{\text{dis}} \text{ yr}^{-1}) = 9.0$ makes sense, that is, a factor of ~ 30 between the CFRs after and inside the age gap. Careful examination of de Grijs & Anders’ (2006) fig. 6a reveals that part of the difference is caused by an underestimate of the slope of their disruption line. While the slope of a constant CFR disruption line is $(1 - \alpha)/\gamma = -1.6$ (Boutloukos & Lamers 2003), their disruption line, obtained from a simple fit to the data, shows a slope of $\simeq -1.8$. As we correct for this effect, the ratio of the CFR 100 Myr ago to that 5 Gyr ago is ~ 20 . In view of the different sampling limits used by de Grijs & Anders (2006) and in this paper, these results (i.e. CFR ratios of 20 and 30) are in reasonable agreement.

As for the CFR at $\simeq 10$ Gyr ago, it is worth bearing in mind that the estimates (3 and 0.5 clusters Myr^{-1} for $\log(t_4^{\text{dis}} \text{ yr}^{-1}) = 9.0$ and 9.9 , respectively) rely thoroughly on the assumption of a power-law ICMF of $\alpha = -2$ for all clusters, irrespective of their age.

Whether the first star clusters to form in the Universe (i.e. globular clusters) are characterised by that ICMF, typical of young star clusters in the Galactic disc and in starbursts and mergers (Zhang & Fall 1999), or by a Gaussian similar to their present-day CMF (Vesperini 1998; Parmentier & Gilmore 2005, 2007) remains a matter of ongoing debate. It is not our aim in this section to discuss the true nature of the ICMF in the LMC 13 Gyr ago. We are prevented from doing so by the paucity of data above the fiducial detection limit at old age. However, it is worth emphasising that the fraction by number of clusters that survive to old age crucially depends on their ICMF. As an illustration, let us assume that $t_4^{\text{dis}} = 2.4$ Gyr. The disruption time-scale of a $10^5 M_\odot$ cluster is then about 10 Gyr (Eq. 2, assuming $\gamma = 0.62$) and all clusters of masses between $10^2 M_\odot$ and $10^5 M_\odot$ will have evaporated by the time their age reaches a Hubble time. If star clusters formed with an ICMF spectral index $\alpha \simeq -2$, this implies a decrease by $\simeq 3$ orders of magnitude in the initial number of clusters. On the other hand, if old LMC clusters formed following the universal Gaussian CMF characteristic of present-day globular cluster systems, clusters more massive than $10^5 M_\odot$ account for about one half of the initial cluster census, thereby implying a survival rate of $\simeq 50$ per cent. Also, the cluster survival rates in

terms of mass and in terms of number are similar in that case (see table 3 in Parmentier & Gilmore 2005 for a comparison of the Galactic halo cluster survival rates in case of power-law and Gaussian ICMFs). Since the survival rates of clusters (in terms of number) at old age depend *heavily* on their ICMF, so does the inferred CFR.

In Fig. 14, we consider the universal globular cluster mass function for the oldest age bin. In other words, in the age range $10.1 < \log(\text{age yr}^{-1}) < 10.2$, we substitute the power-law ICMF of slope $\alpha = -2$ assumed thus far by a Gaussian ICMF with a mean logarithmic cluster mass of 5.3 and a standard deviation of 0.6 dex. At first glance, the evolution of the CFR looks rather noisy. The very low CFR at old age (3 and 1 clusters Gyr^{-1} for $\log(t_4^{\text{dis}} \text{yr}^{-1}) = 9.0$ and 9.9, respectively) is followed by a steep rise amounting to a factor of order 300, which is subsequently succeeded by a 3-fold decrease leading to the age gap.

However, because the CFR is directly determined from the present-day age distribution, they are both affected by the same uncertainties. At ages older than 3 Gyr, the 1σ error bars of the age distribution become significantly larger than at younger ages, as a result of the smaller number of clusters. The CFR at intermediate and old ages becomes similarly uncertain. In order to highlight this, in Fig. 14 we plot the Poissonian error bars of the four oldest bins of the age distribution on the CFR for $\log(t_4^{\text{dis}} \text{yr}^{-1}) = 9.9$. From this simple exercise, it appears that the CFR may have steadily increased from a very low value of about 1 to 3 clusters per Gyr some 15 Gyr ago, up to a 300 – 1000 times higher rate 2 Gyr ago. This steady increase in the CFR is indicated by the thick dashed line in Fig. 14; this is compatible with the four oldest age bins within 1σ .

We therefore conclude that the well-established age gap in the LMC cluster age distribution may not be a faithful mirror of the underlying CFR. This is mainly owing to the assumption that all star clusters were formed in a power-law fashion. For this scenario, the CFR develops a minimum at about 5 Gyr ago, and increases towards both older and younger ages around the age gap (see Fig. 13). However, if the ICMF at the oldest age is different, and similar to the observed Gaussian globular cluster mass function, the resulting bias towards greater cluster mass boosts the number fraction of surviving clusters, thus resulting in a much lower CFR at old age. In the latter case, the CFR has steadily increased over the past Hubble time (see Fig. 14).

Although, in that model, the CFR is increasing by about 2 orders of magnitude from 16 Gyr ago to 8 Gyr ago, the corresponding variations of the formation rate in terms of cluster *mass* are not that significant. Referring to the thick dashed curve in Fig. 14 (i.e. that mimicking the smooth and steady CFR increase with time), the CFR in the last and last but one age bins are $\simeq 1$ cluster per Gyr and $\simeq 50$ clusters per Gyr, respectively. Owing to a different underlying ICMF, these two subsequent age bins are also characterized by markedly different initial mean cluster mass, $\simeq 1000 M_\odot$ for an $\alpha = -2$ power-law ICMF and $\simeq 10^5 M_\odot$ for the universal Gaussian ICMF. Therefore, even though at an age of 10 Gyr the CFR is increasing sharply, the total mass formed in clusters per unit of time is remaining roughly constant, that is, of order $10^2 M_\odot \text{Myr}^{-1}$.

For the sake of completeness, Table 3 lists the initial number of clusters N_{init} and the initial total mass in clus-

Table 3. Initial number of clusters N_{init} and initial total mass in clusters M_{init} required to account for the population of LMC clusters with $7.7 < \log(\text{age yr}^{-1}) < 10.2$. Values are provided for two acceptable cluster disruption time-scales, as well as for two distinct ICMFs for the oldest clusters, either the canonical power-law ("PL") or the universal Gaussian globular cluster mass function ("PL+G_{old}")

ICMF	$\log(t_4^{\text{dis}} \text{yr}^{-1})$	M_{init}	N_{init}
PL	9.0	$60 \times 10^6 M_\odot$	52×10^3
PL	9.9	$18 \times 10^6 M_\odot$	16×10^3
PL+G _{old}	9.0	$46 \times 10^6 M_\odot$	34×10^3
PL+G _{old}	9.9	$17 \times 10^6 M_\odot$	14×10^3

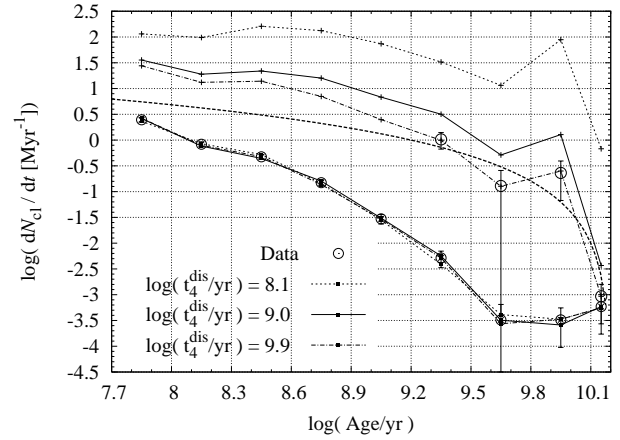


Figure 14. Same as Fig. 13, except for the choice of the ICMF for the oldest age bin: $10.1 < \log(\text{age yr}^{-1}) < 10.2$, for which we assume the universal Gaussian globular cluster mass function. Note how different the predicted CFR at old age is compared to Fig. 13. With an ICMF similar to the universal Gaussian globular cluster mass function, only a few low-mass (say less massive than $10^4 M_\odot$) clusters form, which boosts the cluster survival rate and correspondingly lowers the CFR at old age. Although the temporal evolution of the CFR is rather noisy at old and intermediate ages, it remains consistent (at the 1σ level) with a smooth and steady increase, as shown by the thick dashed line.

ters M_{init} required to account for the census of LMC clusters with $7.7 < \log(\text{age yr}^{-1}) < 10.2$. If the ICMF adopted for the oldest age bin is the observed Gaussian globular cluster mass function (quoted by "PL+G_{old}" in Table 3), the increased cluster survival rate at old age lowers the initial size and the initial total mass of the cluster population, although the effect remains limited owing to the corresponding narrow age range.

While Table 3 builds on a cluster dissolution model with $\gamma = 0.62$, we have also run simulations with $\gamma = 1$ (see section 4 and equations 1 and 2). The size and total mass of the initial cluster population are very much the same if $\log(t_4^{\text{dis}} \text{yr}^{-1}) = 9.9$. By virtue of the weakness of the disruptive processes, the model shows little sensitivity to γ variations. In case of $\log(t_4^{\text{dis}} \text{yr}^{-1}) = 9.0$, the variation in the initial cluster census does not exceed 25 per cent of what we found for $\gamma = 0.62$.

The cluster formation history of the LMC reflects its interaction history with the Small Magellanic Cloud (SMC) and with the Galaxy. This, in turn, is strongly influenced by the orbital evolution of the Magellanic Clouds, which remains poorly known, however. It is still unclear whether the Magellanic Clouds were born initially as a primordial pair of galaxies, or whether they dynamically coupled for the first time some 4 Gyr ago. Besla et al. (2007) re-examine the orbital history of the Clouds on the basis of the most recent proper motion measurements available (Kallivayalil et al. 2006a,b). They find that the existence of a stable binary LMC-SMC system lasting for a Hubble time cannot be precluded, although that remains uncertain. The present status of the orbital history of the Magellanic Clouds about the Galaxy is equally questionable. According to most previous studies, the LMC has completed several pericentric passages about the Galaxy in a Hubble time. Besla et al. (2007) reached the opposite conclusion, however, that the LMC-SMC pair of galaxies may be on their first passage about the Milky Way.

The orbital history of the LMC remains therefore poorly constrained. And so are the origins of the temporal variations of its CFR. Why did it increase from 3 Gyr ago? Whereas Bekki & Chiba (2005) advocate violent and close interactions with the SMC, Besla et al. (2007) favour a scenario in which interactions with the Galaxy are the dominant factor. In fact, the CFR increase from ~ 3 Gyr ago is a natural consequence of their first-passage scenario, as this corresponds to when the Magellanic Clouds first enter inside the virial radius of the Milky Way and begin to interact with the Galactic halo gas.

Finally, we are left with the question as to whether cluster formation in the LMC was in fact reactivated some 3 to 4 Gyr ago (i.e., the ICMF at old age is a power law of spectral index $\alpha = -2$) or whether this increase is merely a continuation of a process started ~ 15 Gyr ago (i.e., the ICMF at old ages is the universal Gaussian globular cluster mass function). A decrease in the CFR from 15 Gyr ago until ~ 5 Gyr ago may be understood in the context of a scenario in which the evolution of the LMC-SMC-Milky Way system is not considered in isolation but, instead, in the wider context of the evolution of the entire Local Group of galaxies. Shuter (1992) and Byrd et al. (1994) considered the possibility that the Magellanic Clouds left the neighbourhood of the Andromeda Galaxy about 10 Gyr ago and were only recently tidally captured by the Milky Way. While recent tidal capture by the Milky Way could have reactivated cluster formation, the decreasing cluster formation rate from the earliest stages may then result from the LMC moving to greater distances from M31. Yet, this scenario is not supported by Besla et al.’s (2007) computations. On the other hand, the steady increase in Fig. 14 may result from the LMC getting closer to the Milky Way, in the context of the first perigalactic passage scenario of Besla et al. (2007). Only future astrometric missions reaching $\sim 10\mu\text{arcsec}$ accuracy can help clarify these issues.

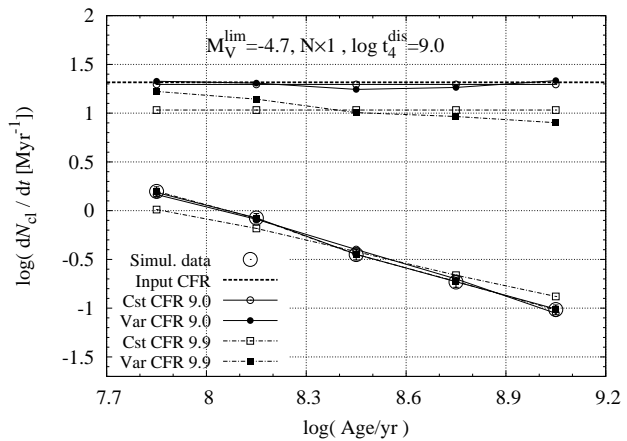


Figure 15. Observed simulations. Simulated data (large open circles) consist of a putative population of star clusters formed with an $\alpha = -2$ power-law ICMF and a constant CFR (indicated by the horizontal thick dashed line) over the age range of the figure. We adopt $t_4^{\text{dis}} = 1$ Gyr and the fiducial detection limit of Fig. 1. The upper lines show the temporal variations of the CFR as derived from the analysis done with the simulated data. Open symbols represent a constant CFR, while filled symbols show CFRs adjusted to match the evolved and observed age distributions. Solid (dash-dotted) lines represent simulations with $\log(t_4^{\text{dis}} \text{yr}^{-1}) = 9.0$ (9.9). Lower lines, identically coded, are the corresponding age distributions.

7 DISENTANGLING THE 1 AND 10 GYR CLUSTER DISRUPTION TIME-SCALES: WHAT KIND OF DATA DO WE MISS ?

In Section 4, we estimated the characteristic disruption time-scale t_4^{dis} of a $10^4 M_\odot$ cluster in the LMC. We concluded that the best constraint we could obtain is a *range* of estimates, i.e. $t_4^{\text{dis}} \geq 1$ Gyr. In other words, despite the proximity of the LMC to the Milky Way, its cluster disruption time-scale cannot be constrained to better than an order of magnitude.

In this section, we investigate which strategy we may adopt in the future to tighten the constraint to the cluster disruption time-scale and, therefore, the cluster formation history in the LMC. Specifically, we generate sets of $(\log(\text{age}), \log(M_{\text{cl}}))$ data, which we subsequently “observe” following the same procedure as before. We can then compare the retrieved (range of) cluster disruption time-scale estimates with the disruption rate actually used to generate these synthetic cluster populations.

Six distinct cases will be discussed. We consider two cluster disruption time-scales ($\log(t_4^{\text{dis}} \text{yr}^{-1}) = 9.0$ and 9.9), combined with three distinct observational situations, in terms of cluster number and detection limit. First, we assume a detection limit and a number of observed clusters similar to that in Section 4 (i.e., $\simeq 400$ clusters brighter than $M_V^{\text{lim}} = -4.7$ mag and spanning the age range [50 Myr, 1.5 Gyr]; labelled “ $M_V^{\text{lim}} = -4.7, N \times 1$ ” in Figs. 15 and 16). Secondly, we retain the same detection limit but consider twice as many clusters (i.e., $\simeq 800$ clusters brighter than $M_V^{\text{lim}} = -4.7$ mag, for $7.7 < \log(\text{age yr}^{-1}) < 9.2$; labelled “ $M_V^{\text{lim}} = -4.7, N \times 2$ ” in Fig. 16). And thirdly, we consider the same number of clusters brighter than $M_V^{\text{lim}} = -4.7$ mag, but a detection limit improved by 1.2 mag, at $M_V^{\text{lim}} = -3.5$ (the fading limit of H03 represented by the

dash-dotted line ‘[3]’ in Fig. 1; labelled “ $M_V^{\text{lim}} = -3.5, N \times 1$ ” in Fig. 16). In the latter case, the total number of clusters is significantly larger because of the inclusion of objects with $-4.7 < M_V < -3.5$ mag.

For the sake of simplicity, we have assumed a constant CFR for $7.4 < \log(\text{age yr}^{-1}) < 9.5$ and the “canonical” $\alpha = -2$ ICMF. After generating ages and masses for the required number of clusters, we added Gaussian noise to our synthetic data set. We adopt $\sigma = 0.15$ dex as the standard deviation of logarithmic cluster ages and masses. This represents a fair upper limit to the internal errors for the de Grijs & Anders (2006) sample, since $\simeq 80$ per cent of their clusters exhibit smaller errors. We then extracted clusters in the appropriate age range and above the appropriate detection limit. Finally, their age distribution integrated over mass, mass distribution integrated over age, and the two-dimensional $(\log(\text{age}), \log(M_{\text{cl}}))$ distribution were analysed in exactly the same way as we did for the observed LMC cluster sample (Section 4).

Figure 15 illustrates the simulated observed age distribution (large open circles) obtained with $\simeq 400$ surviving clusters brighter than the fiducial detection limit at $M_V^{\text{lim}} = -4.7$ in case of $\log(t_4^{\text{dis}} \text{yr}^{-1}) = 9.0$. The upper four lines are the derived CFRs, either constant (open symbols) or adjusted to match the model and observed age distributions (filled symbols). The lower lines, using the same line style coding, are the model age distributions of the detected survivors. Model solutions are shown for two disruption time-scales, $\log(t_4^{\text{dis}} \text{yr}^{-1}) = 9.0$ (circle-symbol lines) and 9.9 (square-symbol lines).

The observed age distribution is well-matched for a constant CFR combined with a cluster disruption time-scale of $\log(t_4^{\text{dis}} \text{yr}^{-1}) = 9.0$, since these are the actual characteristics of the simulated observations. On the other hand, the model based on a constant CFR and $\log(t_4^{\text{dis}} \text{yr}^{-1}) = 9.9$ results in an age distribution (dash-dotted line with open squares) that is shallower than the “observations”. Therefore, on average, the corresponding *adjusted* CFR declines towards older age (dash-dotted line with filled squares).

The input constant CFR used to generate the “observations” is shown as the horizontal thick dashed line (i.e., 20 clusters Myr^{-1}). One can immediately see that, if the cluster disruption time-scale is correctly estimated, the CFR can be derived with great accuracy (i.e., the thick dashed line and the solid line with circles follow each other closely), except for some sampling noise. If the cluster disruption time-scale is incorrectly assumed to be 8 times longer ($\log(t_4^{\text{dis}} \text{yr}^{-1}) = 9.9$), then the CFR is underestimated (as a result of the assumed slow cluster disruption), although by an average factor of two at most.

We now investigate what the conditions are that we need to derive a better approximation to the LMC cluster formation history than what we found in Section 4.

In Fig. 16 we plot the evolution of the $(t_4^{\text{dis}}, \chi_\nu^2)$ functions which follow from the analysis of the simulated data. In the left and right-hand panels, the simulated star cluster evolution is characterised by $\log(t_4^{\text{dis}} \text{yr}^{-1}) = 9.0$ and 9.9, respectively. $[\chi_\nu^2]_{\text{MF}}$ and $[\chi_\nu^2]_{\text{GRID}}$ are the reduced χ_ν^2 derived from the CMF integrated over age, and from the two-dimensional $(\log(\text{age}), \log(M_{\text{cl}}))$ distribution of clusters, respectively.

For an observational situation similar to that discussed

in this paper (dotted line), we see that the cluster disruption time-scale is rather loosely constrained. In none of the panels does the $(t_4^{\text{dis}}, \chi_\nu^2)$ function show a clear minimum. For instance, let us consider the third panel from the top in the left column of Fig. 16 (i.e., the $[\chi_\nu^2]_{\text{MF}}$ obtained for an adjusted CFR – ‘Var CFR’). It shows that $[\chi_\nu^2]_{\text{MF}, \text{min}} \simeq 1$ at $\log(t_4^{\text{dis}} \text{yr}^{-1}) = 8.9$ and $[\chi_\nu^2]_{\text{MF}} < [\chi_\nu^2]_{\text{MF}, \text{min}} + 1$ for $8.6 \leq \log(t_4^{\text{dis}} \text{yr}^{-1}) \leq 9.7$. We therefore recover the correct cluster disruption time-scale ($\log(t_4^{\text{dis}} \text{yr}^{-1}) = 9.0$), but the range of acceptable estimates covers a decade in t_4^{dis} . Even if the detection limit remains the same, that situation is improved if the number of clusters in the sample is increased. With twice as many clusters, one now obtains $[\chi_\nu^2]_{\text{MF}, \text{min}} \simeq 1$ at $\log(t_4^{\text{dis}} \text{yr}^{-1}) = 8.9$ and $[\chi_\nu^2]_{\text{MF}} < [\chi_\nu^2]_{\text{MF}, \text{min}} + 1$ for $8.7 \leq \log(t_4^{\text{dis}} \text{yr}^{-1}) \leq 9.4$ (solid curve). The uncertainties on $\log(t_4^{\text{dis}})$ are now reduced by a factor of about two, as a direct result of the smaller Poissonian noise in the cluster age and mass distributions. In other words, the more populous a star cluster system is, the better its inferred cluster formation history.

The best accuracy for the t_4^{dis} estimate is achieved when the detection limit gets fainter by 1.2 mag (dashed curve). In that case, $[\chi_\nu^2]_{\text{MF}, \text{min}} \simeq 1.4$ at $\log(t_4^{\text{dis}} \text{yr}^{-1}) = 9.1$ and $[\chi_\nu^2]_{\text{MF}} < [\chi_\nu^2]_{\text{MF}, \text{min}} + 1$ for $8.8 \leq \log(t_4^{\text{dis}} \text{yr}^{-1}) \leq 9.35$. If we compare this with the right-hand equivalent panel in Fig. 16, for which $\log(t_4^{\text{dis}} \text{yr}^{-1}) = 9.9$, we find $[\chi_\nu^2]_{\text{MF}, \text{min}} \simeq 0.3$ for $\log(t_4^{\text{dis}} \text{yr}^{-1}) \geq 9.7$ and $[\chi_\nu^2]_{\text{MF}} < [\chi_\nu^2]_{\text{MF}, \text{min}} + 1$ for $\log(t_4^{\text{dis}} \text{yr}^{-1}) \geq 9.4$. We therefore conclude that if the star cluster system of the LMC were observed with a 90 per cent completeness limit of $M_V \simeq -3.5$ mag, we could decide more easily whether the cluster disruption time-scale is of order 1 or 10 Gyr, which we cannot do with the data presently available to us.

The reason why a detection limit improved by $\Delta \log(M_{\text{cl}}/M_\odot) \simeq -0.5$ better distinguishes $\log(t_4^{\text{dis}} \text{yr}^{-1}) = 9.0$ from 9.9 is directly related to whether or not the turn-over expected to appear in the CMF as a result of dynamical secular evolution shows up above the detection limit. To illustrate this, we carried out additional simulations, the results of which we show in Fig. 17.

Each panel of Fig. 17 corresponds to a synthetic star cluster population formed with a constant CFR for the given age range, and with the “canonical” ($\alpha = -2$) power-law ICMF. Here, we are interested in the location of the CMF turn-over with respect to the detection limit, independently of the presence of observational errors and of size-of-sample related Poissonian noise. To limit this, we adopt a fairly large initial number of clusters (4×10^5) for each limited age range (i.e., for each panel). The cluster disruption time-scale is $\log(t_4^{\text{dis}} \text{yr}^{-1}) = 9.0$ and 9.9 in the left and right-hand panels, respectively. The dashed line represents the ICMF and the solid line is for the evolved CMF for the age ranges considered, i.e., from top to bottom: $7.7 < \log(\text{age yr}^{-1}) < 8.0$, $8.3 < \log(\text{age yr}^{-1}) < 8.6$, $8.9 < \log(\text{age yr}^{-1}) < 9.2$, and $9.5 < \log(\text{age yr}^{-1}) < 9.8$. Also shown are the detection limits corresponding to $M_V^{\text{lim}} \simeq -4.7$ mag (vertical thick solid line) and to $M_V^{\text{lim}} \simeq -3.5$ mag (vertical thick dotted line), which we discussed above.

At young ages ($7.7 < \log(\text{age yr}^{-1}) < 8.0$), the evolved CMF remains a good proxy to the ICMF. As clusters age, the power-law ICMF is secularly turned into a Gaussian CMF. The older the cluster system and/or the shorter t_4^{dis} ,

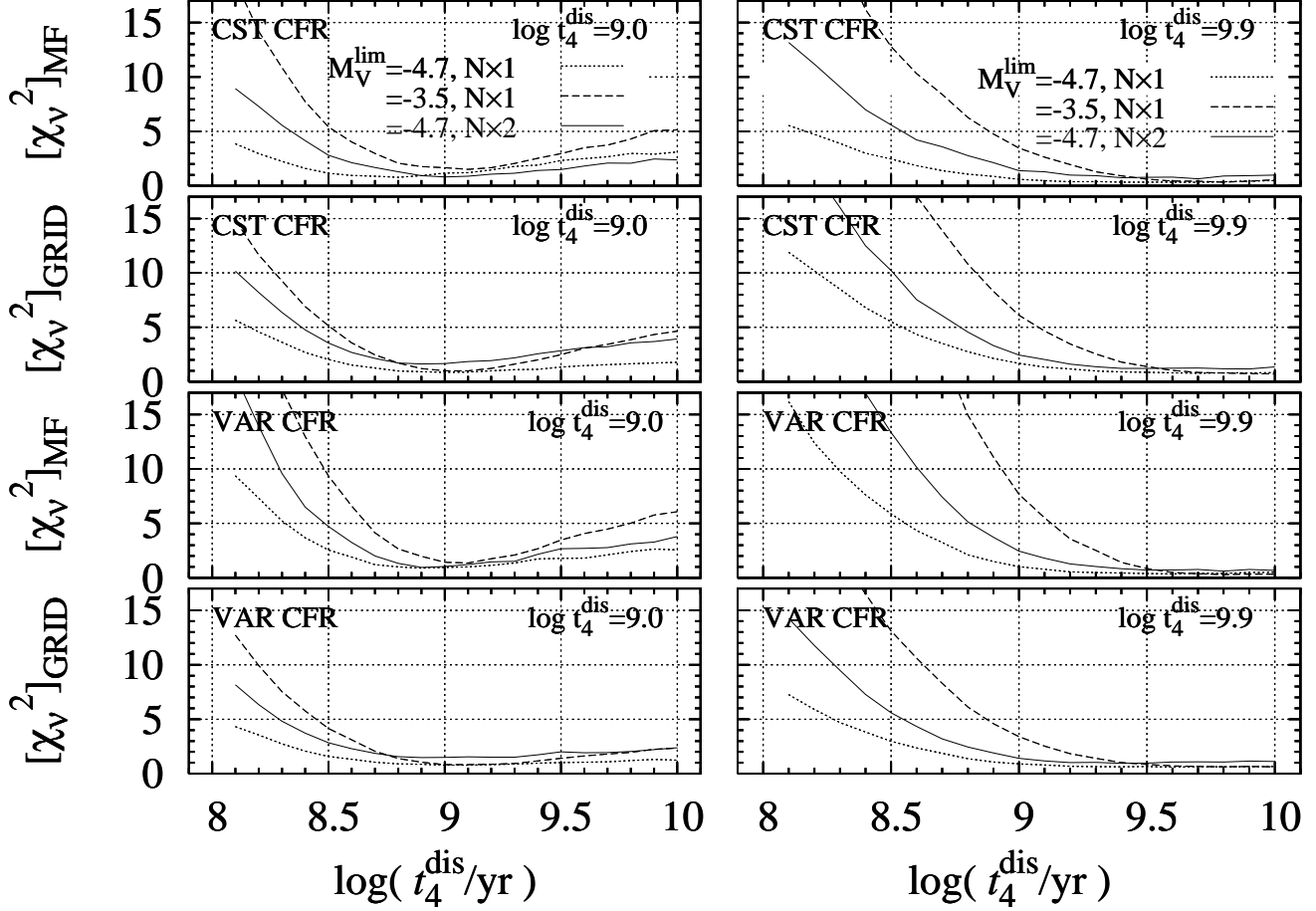


Figure 16. Results of χ^2 tests done for synthetic star cluster populations. These are formed with a constant CFR, the “canonical” power-law ICMF ($\alpha = -2$), and cluster disruption time-scales of $\log(t_4^{\text{dis}} \text{yr}^{-1}) = 9.0$ and 9.9 in the left and right-hand panels, respectively. Following the addition of Gaussian noise to $\log(M_{\text{cl}})$ and $\log(\text{age})$ of the survivors (to mimic an observational situation), clusters with $7.7 < \log(\text{age yr}^{-1}) < 9.2$ and located above a detection limit of either $M_V^{\text{lim}} = -4.7$ mag (solid and dotted lines) or $M_V^{\text{lim}} = -3.5$ mag (dashed line) are extracted from the generated files and processed by the same method as used in Section 4 for the LMC data. The resultant χ^2 functions are shown. Dotted lines correspond to a star cluster system including about 380 clusters brighter than $M_V^{\text{lim}} = -4.7$ mag (cf. Section 4). Solid lines illustrate how χ^2 functions improve should the cluster census be doubled, all other parameters being kept the same. The dashed lines show the accuracy of the cluster disruption time-scale that is to be expected if the LMC cluster sample were complete above $M_V^{\text{lim}} = -3.5$ mag.

the higher the resulting cluster mass at the turn-over. Let us consider the left-hand panels, for which $\log(t_4^{\text{dis}} \text{yr}^{-1}) = 9.0$. At an age of 1 Gyr, the turn-over remains at the lower edge of the fiducial detection limit of $M_V^{\text{lim}} \simeq -4.7$ mag. As a result, the imprint of dynamical evolution is barely detectable and t_4^{dis} cannot be determined from the turn-over location. All we can retrieve is a lower limit to t_4^{dis} , in the sense that we can exclude all disruption time-scales which are short enough to bring the CMF turn-over beyond the detection limit. With the improved detection limit of $M_V^{\text{lim}} \simeq -3.5$ mag (vertical dotted line), the cluster mass at the turn-over is (just) measurable, hence the clear minimum seen in the $[\chi_v^2]_{\text{MF}}$ of the third panel on the left-hand side in Fig. 16 (dashed line). If $\log(t_4^{\text{dis}} \text{yr}^{-1}) = 9.9$, however, the CMF evolves on such a slow time-scale that the turn-over remains undetected, regardless of whether $M_V^{\text{lim}} \simeq -3.5$ or -4.7 mag. Only a lower limit to $\log(t_4^{\text{dis}} \text{yr}^{-1})$ can be inferred and the χ^2 functions are steadily decreasing with increasing t_4^{dis} (right-hand panels of Fig. 16).

We note in passing that deriving a t_4^{dis} estimate rather than a lower limit is better achievable based on a more evolved cluster population, if either the cluster disruption time-scale is shorter or if the population contains older clusters. As for the latter, this is so because disruption limits in $(\log(\text{age}), \log(M_{\text{cl}}))$ space (dashed lines in Fig. 1) are steeper than detection limits (dash-dotted lines in Fig. 1). Yet, in that case, the small number of survivors at old age, where the turn-over location is firmly set, may hamper any analysis as a result of significant Poissonian noise (see, e.g., the fourth panel on the left-hand side in Fig. 17).

Our LMC star cluster sample lacks clusters at intermediate and old age, as it contains only $\simeq 20$ star clusters older than 1 Gyr above the fiducial detection limit. Combined with the bright fiducial detection limit we defined in Section 3, this data paucity results in only a lower limit to the characteristic LMC star cluster disruption time-scale of $t_4^{\text{dis}} \geq 1$ Gyr.

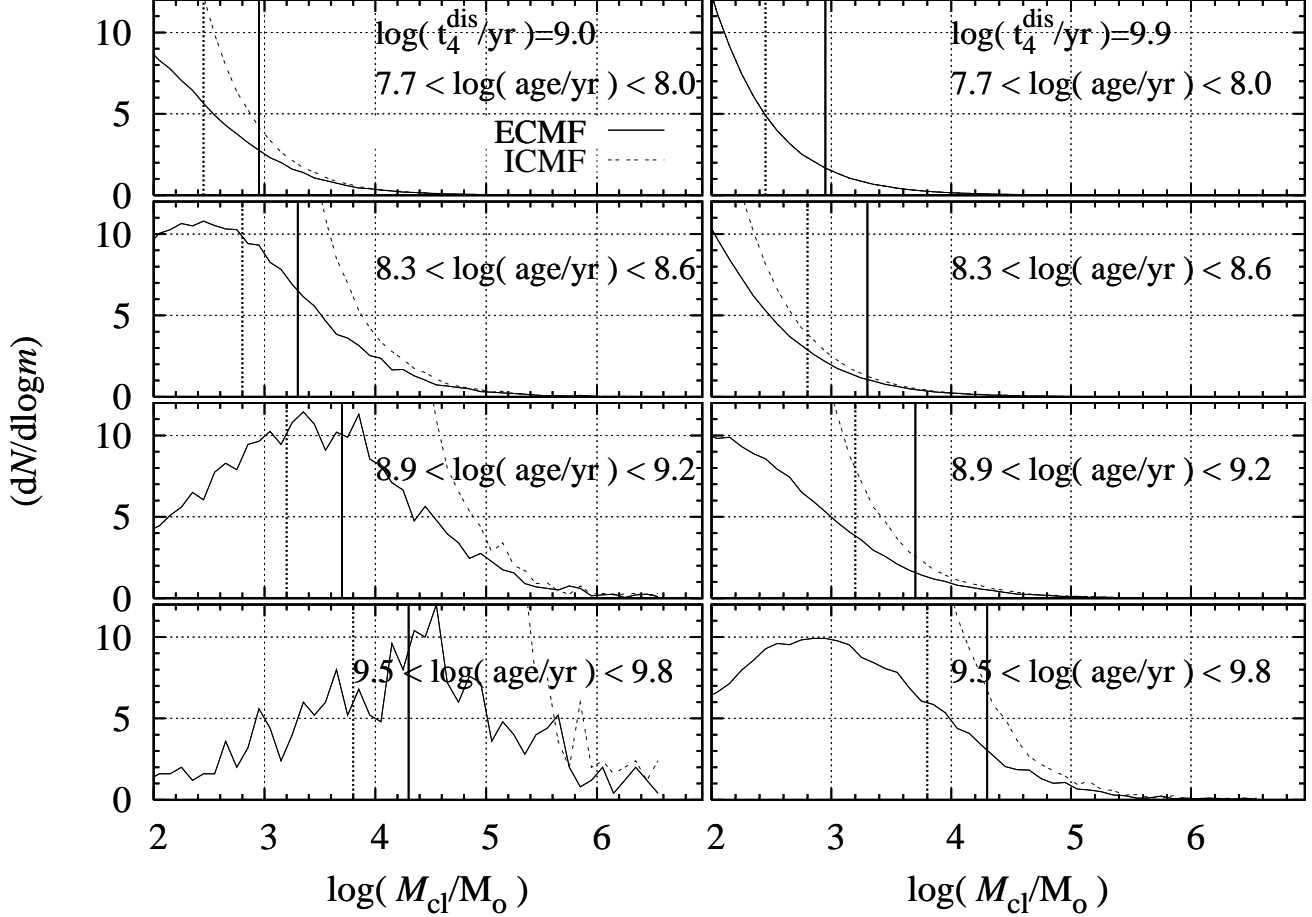


Figure 17. Evolved CMFs (solid lines) of synthetic star cluster populations formed with a constant CFR, a power-law ICMF of spectral index $\alpha = -2$ (dashed lines), and two cluster disruption time-scales of $\log(t_4^{\text{dis}}/\text{yr}) = 9.0$ and 9.9 (left and right-hand panels, respectively). Different age ranges (listed in each panel) are displayed. The vertical solid and dashed lines represent detection limits at $M_V^{\text{lim}} = -4.7$ mag (fiducial detection limit; thick dash-dotted line with symbols in Fig. 1) and $M_V^{\text{lim}} = -3.5$ mag (thin dash-dotted line labelled ‘[3]’ in Fig. 1). As secular evolution proceeds, the turn-over in mass of the dynamically-shaped CMF shifts towards higher cluster masses and the number of surviving clusters steadily declines, thereby enhancing the presence of sampling noise in the CMF. The vertical scaling is arbitrary.

8 SUMMARY AND CONCLUSIONS

In this paper, we have carried out numerous detailed Monte-Carlo simulations aimed at constraining the cluster formation history and the rate of bound cluster disruption in the LMC star cluster system. We considered only clusters older than 50 Myr in order not to determine erroneously short cluster disruption time-scale as a result of the inclusion of the infant mortality and infant weight loss evolutionary phases. Our data are based on the *UBVR* photometry of H03 (obtained from Massey’s (2002) survey of the Magellanic Clouds), for which de Grijs & Anders (2006) obtained homogeneously determined age and mass estimates. We estimated a fiducial detection limit above which the cluster sample is (fairly) complete from the CMF as a function of age, at $M_V^{\text{lim}} = -4.7$ mag. This is significantly brighter than H03’s fading limit. We consider only clusters brighter than this limit, in order to avoid severe statistical incompleteness effects.

We have evolved synthetic star cluster systems characterised by constant CFRs assuming 20 different cluster

disruption time-scales. The CFR was adjusted to reproduce the observed age distribution. By doing so, we are likely to loose sensitivity to CFR variations occurring on a time-scale shorter than the width of the age range corresponding to each logarithmic age bin (i.e., more likely at old age where our age bins span greater linear age ranges than at young age). However, the general behaviour of the CFR, as well as the CFR averaged over age are robustly recovered (see Section 7). We then compare, in a “Poissonian” χ^2 sense the modelled mass distribution and the modelled $[\log(\text{age}), \log(M_{\text{cl}})]$ distribution to the observations. We show that because of the bright detection limit at $M_V^{\text{lim}} = -4.7$ mag, one cannot constrain t_4^{dis} to better than a lower limit, $t_4^{\text{dis}} \geq 1$ Gyr. The tightest constraints are set by the CMF integrated over age. The χ^2 test applied to the distribution of points in $[\log(\text{age}), \log(M_{\text{cl}})]$ space turns out to be a poor diagnostic tool. This is probably related to the low density of points in each cell of the $[\log(\text{age}), \log(M_{\text{cl}})]$, compared to the density of points in each bin of the integrated CMF, leading to smaller Poissonian error bars and therefore a better constrained model in the latter case. Our

range of cluster disruption time-scale estimates is robust with respect to model variations, such as of the upper limit of the initial cluster mass range, the location of the grid in $[\log(\text{age}), \log(M_{\text{cl}})]$, and the size of cells in this grid.

We have shown that should the detection limit be underestimated, artificially shortened cluster disruption time-scales would result. This is so because there is a degeneracy between incompleteness and secular evolution, i.e., the fading-driven turn-over in a CMF in a given age bin is interpreted as resulting from secular evolution, leading to a shortened cluster disruption time-scale.

Having set the best possible constraints on t_4^{dis} , we explored the corresponding CFR, in particular considering $t_4^{\text{dis}} = 1$ and 10 Gyr. The CFR has been increasing steadily from about 0.3 clusters Myr^{-1} 5 Gyr ago, to a present rate of (20 – 30) clusters Myr^{-1} , for clusters spanning an initial mass range of $\sim 100 - 10^7 M_{\odot}$. The CFRs inferred for both disruption time-scales differ by at most a factor of three (Fig. 13). At older ages however, the situation becomes unclear. The uncertainty in the CFR as a result of the uncertainty on t_4^{dis} increases. In addition, the overall temporal behaviour of the CFR depends on the shape of the ICMF of the oldest, globular cluster-like objects. If this is the universal Gaussian ICMF, then the CFR has increased steadily over a Hubble time from ~ 1 cluster Gyr^{-1} 15 Gyr ago to its present value. On the contrary, if the ICMF has always been a power law with a slope close to $\alpha = -2$, the CFR exhibits a minimum some 5 Gyr ago. Our results may be related to the orbital history and dynamics of the LMC with respect to both the SMC and the Milky Way, although this remains poorly constrained because of a lack of proper motion measurements with the required accuracy (Besla et al. 2007).

Additionally, we note that interactions between the Clouds and between the Clouds and the Galaxy, while affecting their star-formation history, also affect the *structure* of the Magellanic Clouds (Bekki & Chiba 2005). This may have induced temporal variations in the cluster disruption time-scale over the past Hubble time, rendering the cluster disruption time-scale estimate at old age even more uncertain.

Finally, we have investigated which strategy should be adopted in the future in order to better constrain the cluster disruption time-scale in the LMC. Specifically, we have generated synthetic cluster populations defined by a given cluster formation history, ICMF and various dissolution rates. After the addition of Gaussian noise to mimic an observational situation, we processed these simulated data sets in the same way as the actual LMC data. We demonstrate that *if* the cluster disruption time-scale is known, then the CFR can be derived accurately. We confirm our inability to distinguish $t_4^{\text{dis}} = 1$ Gyr from 10 Gyr because of the bright detection limit. With such a bright detection limit, the expected turn-over in the CMF caused by dynamical evolution is not detected, for any cluster age range. As a result, only a lower limit to the cluster disruption time-scale can be retrieved, i.e., we can exclude all t_4^{dis} that are short enough to lead to a turn-over above the detection limit. To obtain age and mass estimates for an LMC star cluster sample complete above $M_V^{\text{lim}} = -3.5$ is desirable to more easily distinguish between $t_4^{\text{dis}} = 1$ Gyr and $t_4^{\text{dis}} = 10$ Gyr.

ACKNOWLEDGMENTS

We thank Peter Anders for helpful discussions and for performing the broad-band SED analysis resulting in the cluster age and mass determinations used in this paper. GP acknowledges support from the Belgian Science Policy Office in the form of a Return Grant and from the Alexander von Humboldt Foundation in the form of a Research Fellowship. We are grateful for research support and hospitality at the International Space Science Institute in Bern (Switzerland), as part of an International Team Programme. We acknowledge partial financial support from the UK's Royal Society through an International Joint Project grant aimed at facilitating networking activities between the universities of Sheffield and Bonn. This research has made use of NASA's Astrophysics Data System Abstract Service.

REFERENCES

- Anders P., Bissantz N., Fritze-v. Alvensleben U., de Grijs R., 2004, MNRAS, 347, 196
- Bastian N., Gieles M., Lamers H.J.G.L.M., Scheepmaker R.A., de Grijs R. 2005, A&A 431, 905
- Bastian N., Goodwin S. P., 2006, MNRAS, 369, L9
- Battinelli P., Brandimarti A., Capuzzo-Dolcetta R., 1994, A&AS, 104, 379
- Baumgardt H., 1998, A&A, 330, 480
- Baumgardt H., Makino J., 2003, MNRAS, 340, 227
- Bekki K., Chiba M., 2005, MNRAS, 356, 680
- Besla G., Kallivayalil N., Hernquist L., Robertson B., Cox T. J., van der Marel R. P., Alcock C., 2007, (arXiv:astro-ph/0703196)
- Bik A., Lamers H. J. G. L. M., Bastian N., Panagia N., Romaniello M., 2003, A&A, 397, 473
- Byrd G., Valtonen M., McCall M., Innanen K., 1994, AJ, 107, 2055
- Anders P., Bissantz N., Boysen L., de Grijs R., Fritze-v. Alvensleben U., 2007, MNRAS, 377, 91
- Anders P., Fritze-v. Alvensleben U., 2003, A&A, 401, 1063
- Bica E. L. D., Schmitt H. R., Dutra C. M., Oliveira H. L., 1999, AJ, 117, 238
- Boutloukos S. G., Lamers H. J. G. L. M., 2002, in: Extragalactic Star Clusters, IAU Symp. 207, Geisler D., Grebel E. K., Minniti D., (San Francisco: ASP), p.703
- Boutloukos S. G., Lamers H. J. G. L. M., 2003, MNRAS, 338, 717
- Calzetti D., 1997, AJ, 113, 162
- Calzetti D., Armus L., Bohlin R. C., Kinney A. L., Koornneef J., Storchi-Bergmann T., 2000, ApJ, 533, 682
- Calzetti D., 2001, PASP, 113, 1449
- Cardelli J. A., Clayton G. C., Mathis J. S., 1989, ApJ, 345, 245
- de Grijs R., Bastian N., Lamers H. J. G. L. M., 2003a, MNRAS, 340, 197
- de Grijs R., Fritze-v. Alvensleben U., Anders P., Gallagher J. S. III, Bastian N., Taylor V. A., Windhorst R. A., 2003b, MNRAS, 342, 259
- de Grijs R., Anders P., Lynds R., Bastian N., Lamers H. J. G. L. M., O'Neill E. J., Jr., 2003c, MNRAS, 343, 1285
- de Grijs R., Anders P., Lamers H. J. G. L. M., Bastian N., Parmentier G., Sharina M. E., Yi S., 2005, MNRAS, 359, 874
- de Grijs R., Parmentier G., Lamers H. J. G. L. M., 2005, MNRAS, 364, 1054
- de Grijs R., Anders P., 2006, MNRAS, 366, 295
- de Grijs R., Parmentier G., 2007, ChJA&A, 7, 155
- de Grijs R., Goodwin S. P., 2007, MNRAS (letters), submitted
- Dolphin A. E., 2002, MNRAS, 332, 91

- Dolphin A. E., Kennicutt R. C., Jr., 2002, *AJ*, 124, 158
- Fall S.M., Chandar R., Whitmore B.C., 2005, *ApJL*, 631, 133
- Fall S.M., 2006, *ApJ*, 652, 1129
- Gieles M., Bastian N., Lamers H. J. G. L. M., Mout J. N., 2005, *A&A*, 441, 949
- Gieles M., 2007, in: proceedings of Mass loss from stars and the evolution of stellar clusters, A. de Koter, R. Waters, L. Smith (eds), ASP Conference Series, in press (arXiv:0702267)
- Goodwin S. P., Bastian N., 2006, *MNRAS*, 373, 752
- Hunter D. A., Elmegreen B. G., Dupuy T. J., Mortonson M., 2003, *AJ*, 126, 1836 (H03)
- Kallivayalil N., van der Marel R. P., Alcock C., Axelrod T., Cook K. H., Drake A. J., Geha M., 2006a, *ApJ*, 638, 772
- Kallivayalil N., van der Marel R. P., Alcock C., 2006b, *ApJ*, 652, 1213
- Kroupa P., Boily C., 2004, *ANS*, 325, 34
- Kurth O. M., Fritze-v. Alvensleben U., Fricke K. J., 1999, *A&AS*, 138, 19
- Lada C. J., Lada E. A., 2003, *ARA&A*, 41, 57
- Lamers H. J. G. L. M., Gieles M., Bastian N., Baumgardt H., Kharchenko N. V., Portegies Zwart S., 2005a, *A&A*, 441, 117
- Lamers H. J. G. L. M., Gieles M., Portegies Zwart S. F., 2005b, *A&A*, 429, 173
- Leitherer C., Li I.-H., Calzetti D., Heckman T. M., 2002, *ApJS*, 140, 303
- Massey P., 2002, *ApJS*, 141, 81
- McLaughlin D. E., 1999, *AJ*, 117, 2398
- Mengel S., Lehnert M. D., Thatte N., Genzel R., 2005, *A&A*, 443, 41
- Parmentier G., Gilmore G., 2005, *MNRAS*, 363, 326
- Parmentier G., Gilmore G., 2007, *MNRAS*, 377, 352
- Pietrzyński G., Udalski A., Kubiak M., Szymański M., Woźniak P., Żebruń K., 1999, *AcA*, 49, 521
- Schlegel D.J., Finkbeiner D. P., Davis M., 1998, *ApJ*, 500, 525
- Schulz J., Fritze-v. Alvensleben U., Möller C. S., Fricke K. J., 2002, *A&A*, 392, 1
- Shuter W. L. H., 1992, *ApJ*, 386, 101
- Smith L.J., Bastian N., Konstantopoulos I.S., Gallagher J.S., Gieles M., de Grijs R., Larsen S.S., O'Connell R.W., Westmoquette M.S., 2007, *ApJL* (in press), arXiv0708.0814v1
- Vesperini E., 1998, *MNRAS*, 299, 1019
- Waters C.Z., Zepf, S.E., Lauer T.R., Baltz E.A., Silk J., 2006, *ApJ*, 650, 885
- Weidner C., Kroupa P., Nürnberger D. E. A., Sterzik M. F., 2007, *MNRAS*, 376, 1879
- Zhang Q., Fall S. M., 1999, *ApJ*, 527, L81

